tRNA-derived fragment tRF-1^{ArgACG} drives HCC osteolytic bone metastasis via ALKBH5-mediated INPP4B destabilization and PI3K/AKT activation

Jinyan Feng[1*], Long Chen[1,4*], Xianfu Wei[1,3*], Houzhi Yang[1*], Xiuxin Han[1], Qingqian Zhao[1], Qian Li[1], Xin Chen[2], Chao Zhang[1], Yafei Wang[5#], Bowen Liu[2#], Guowen Wang[1#]

[1]National Key Laboratory of Druggability Evaluation and Systematic Translational Medicine, Tianjin's Clinical Research Center for Cancer, Department of Bone and Soft Tissue Tumors, Tianjin Medical University Cancer Institute and Hospital, National Clinical Research Center for Cancer, Tianjin, 300060, China.

[2]Xinxiang Key Laboratory of Inflammation and Immunology, School of Medical Technology, Xinxiang Medical University, Xinxiang, Henan 453003, China.

[3]Department of Orthopedics, Qilu Hospital of Shandong University, Jinan, Shandong, 250012, China.

[4]Department of Musculoskeletal Oncology, Clinical Oncology School of Fujian Medical University, Fujian Cancer Hospital, Fuzhou 350000, China.

[5]Department of Hematology, Tianjin Medical University Cancer Institute and Hospital, National Clinical Research Center for Cancer, Key Laboratory of Cancer Prevention and Therapy, Tianjin's Clinical Research Center for Cancer, Tianjin, 300060, China.

*Jinyan Feng, Long Chen, Xianfu Wei and Houzhi Yang have contributed equally to this work

[#]Correspondence: Guowen Wang, E-mail: wangguowen@tmu.edu.cn. Bowen Liu, E-mail: liubowen309@163.com. Yafei Wang, E-mail: drwang2005@163.com. Department of Bone and Soft Tissue Tumors, Tianjin Medical University Cancer Institute and Hospital, Huanhu Xi Road, Tiyuan Bei, Hexi District, Tianjin 300060, P.R. China, Phone: +86-18802237773.

Supplementary figures and legends

Figure S1

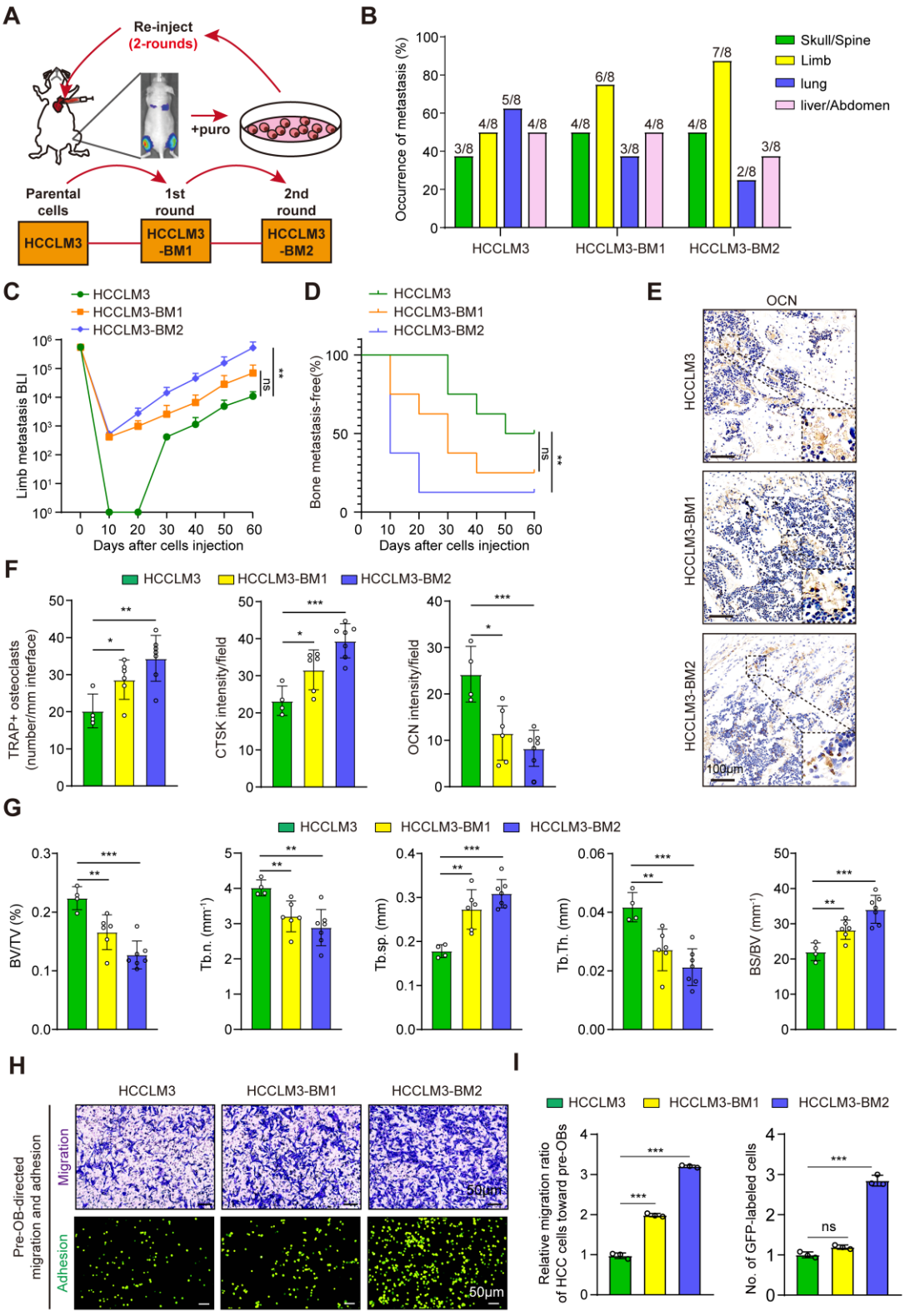
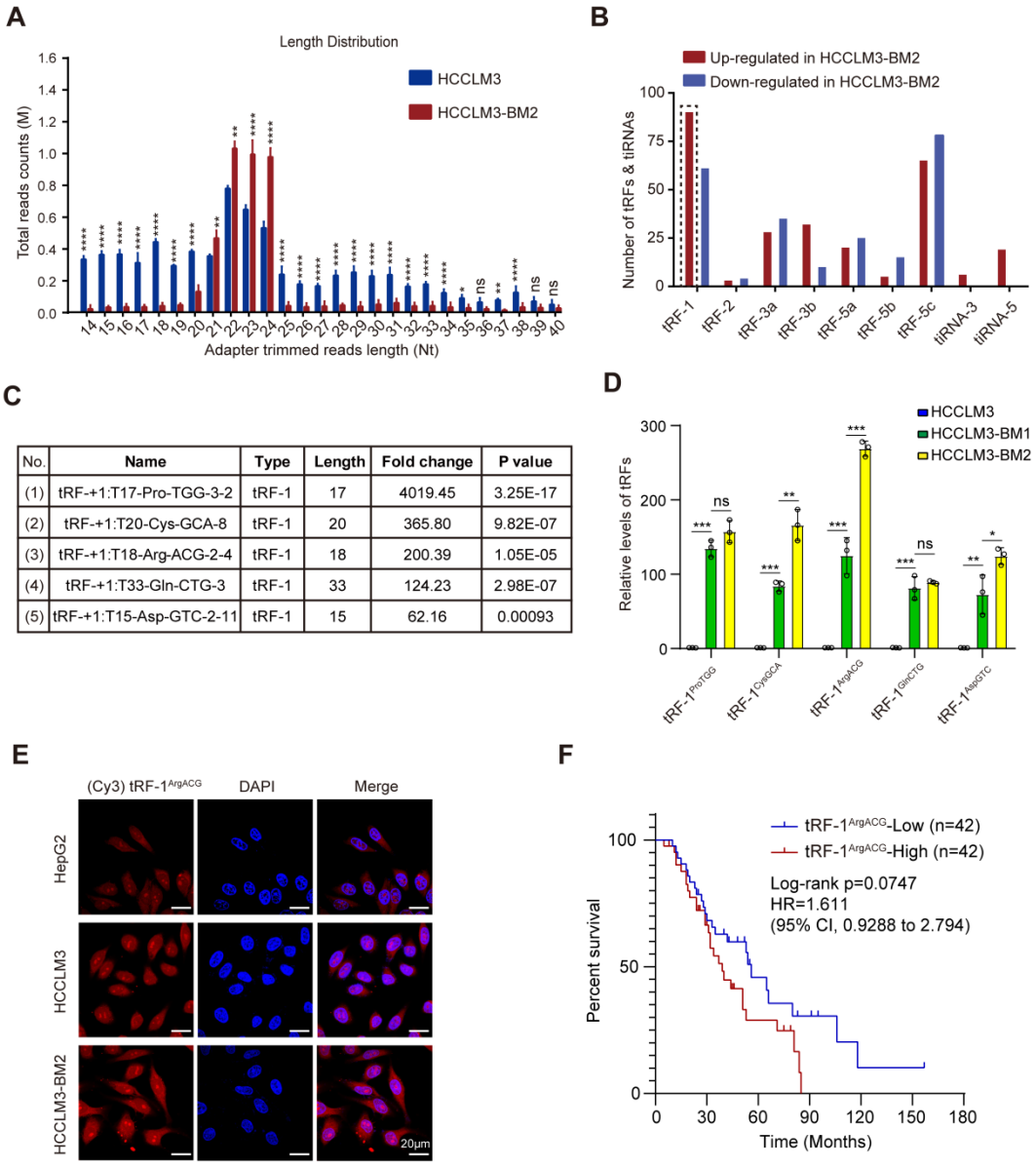


Figure S1. Establishment and characterization of bone-metastatic HCCLM3 sublines.

(A) Schematic illustration of the serial in vivo selection strategy used to establish HCCLM3-BM1 and HCCLM3-BM2 cells. HCCLM3 cells were intracardially inoculated into mice, and tumor cells isolated from skeletal metastatic lesions were expanded in vitro and subjected to two successive rounds of skeletal selection. (B) Incidence of metastases to the skull/spine, limbs, lungs, and liver/abdomen following intracardiac inoculation of HCCLM3, HCCLM3-BM1, or HCCLM3-BM2 cells (n=8 successfully inoculated mice per group). (C) Longitudinal quantification of limb metastatic BLI signals in mice inoculated with HCCLM3, HCCLM3-BM1, or HCCLM3-BM2 cells. (D) Kaplan–Meier curves showing bone metastasis-free survival in the indicated groups. (E) Representative OCN immunohistochemical staining of bone lesions from the indicated groups (scale bar, 100 μm). (F) Quantification of TRAP+ osteoclasts and CTSK and OCN staining in bone lesions from the indicated groups. (G) Quantitative micro-CT analysis of BV/TV, Tb.N, Tb.Sp, Tb.Th, and BS/BV in the indicated groups. (H, I) Representative images (H) and quantification (I) of Pre-OB-directed migration and adhesion assays in HCCLM3, HCCLM3-BM1, and HCCLM3-BM2 cells (scale bars, 50 μm). Data are presented as mean ± SD. *$P < 0.05$; **$P < 0.01$; ***$P < 0.001$; ns, not significant.

Figure S2



No.	Name	Type	Length	Fold change	P value
(1)	tRF-+1:T17-Pro-TGG-3-2	tRF-1	17	4019.45	3.25E-17
(2)	tRF-+1:T20-Cys-GCA-8	tRF-1	20	365.80	9.82E-07
(3)	tRF-+1:T18-Arg-ACG-2-4	tRF-1	18	200.39	1.05E-05
(4)	tRF-+1:T33-Gln-CTG-3	tRF-1	33	124.23	2.98E-07
(5)	tRF-+1:T15-Asp-GTC-2-11	tRF-1	15	62.16	0.00093

Figure S2. Characterization and clinical association of tRF-1^{ArgACG} in HCC. (A) tRF/tiRNA length distribution profiles in HCCLM3 and HCCLM3-BM2 cells. (B) Numbers of significantly upregulated and downregulated tRFs/tiRNAs according to tRF/tiRNA subtype in HCCLM3-BM2 cells relative to HCCLM3 cells. (C) Top five upregulated tRF-1 candidates in HCCLM3-BM2 cells ranked by fold change. (D) tRF-qPCR validation of the five candidate tRFs in HCCLM3, HCCLM3-BM1, and HCCLM3-BM2 cells. (E) Subcellular localization of tRF-1^{ArgACG} detected by FISH analysis in HepG2, HCCLM3, and HCCLM3-BM2 cells using Cy3-labeled probes (red); nuclei were counterstained with DAPI

(blue) (scale bars, 20 μm). (F) Kaplan-Meier analysis of OS in HCC patients stratified by high or low tRF-1^{ArgACG} expression in our clinical cohort using the cohort-specific median staining score of 3.285 as the cut-off (n=84; high, n=42; low, n=42; HR = 1.611, 95% CI: 0.9288–2.794; log-rank P = 0.0747). Data are presented as mean ± SD where applicable. *P < 0.05; **P < 0.01; ***P < 0.001; ****P < 0.0001. ns, not significant.

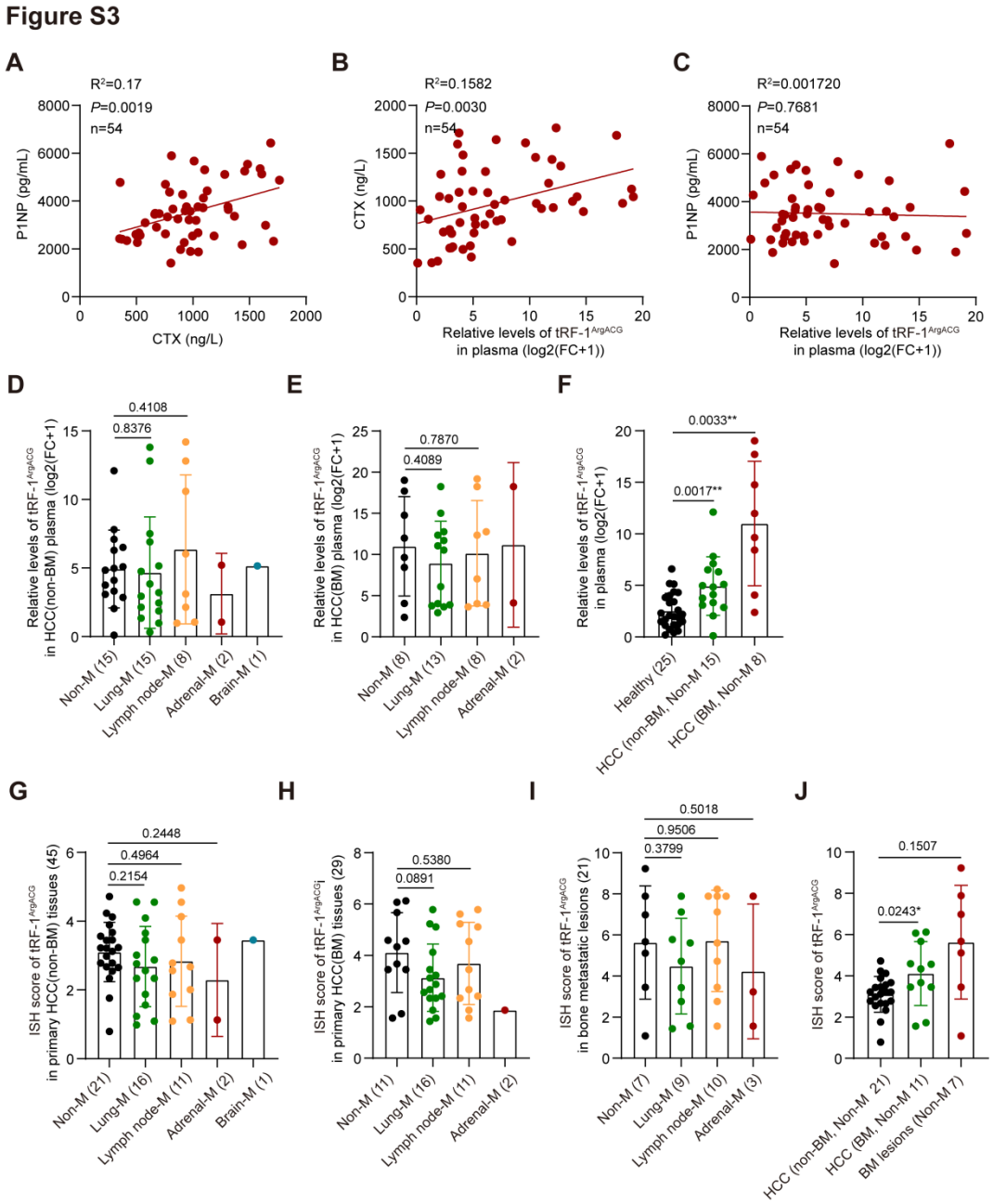


Figure S3. Association of tRF-1^{ArgACG} with bone turnover markers and metastatic involvement in patients with HCC. (A) Pearson correlation analysis between serum CTX and P1NP levels in patients with HCC (n=54). (B) Pearson correlation analysis between

plasma tRF-1^{ArgACG} levels and serum CTX levels in patients with HCC (n=54). (C) Pearson correlation analysis between plasma tRF-1^{ArgACG} levels and serum P1NP levels in patients with HCC (n=54). (D) Plasma tRF-1^{ArgACG} levels in HCC patients without bone metastasis, stratified according to the presence of lung, lymph node, adrenal, or brain metastases. (E) Plasma tRF-1^{ArgACG} levels in HCC patients with bone metastasis, stratified according to the presence of lung, lymph node, or adrenal metastases. (F) Plasma tRF-1^{ArgACG} levels in healthy donors (n=25), HCC patients without bone metastasis and without other metastases (n=15), and HCC patients with bone metastasis and without other metastases (n=8). (G) tRF-1^{ArgACG} ISH scores in primary HCC tissues from patients without bone metastasis, stratified according to the presence of lung, lymph node, adrenal, or brain metastases. (H) tRF-1^{ArgACG} ISH scores in primary HCC tissues from patients with bone metastasis, stratified according to the presence of lung, lymph node, or adrenal metastases. (I) tRF-1^{ArgACG} ISH scores in bone-metastatic lesions, stratified according to the presence of lung, lymph node, or adrenal metastases. (J) tRF-1^{ArgACG} ISH scores in primary HCC tissues without bone metastasis (n=21), primary HCC tissues with bone metastasis (n=11), and bone-metastatic lesions (n=7) from patients without other metastases. Data are presented as mean ± SD where applicable. *$P < 0.05$; **$P < 0.01$.

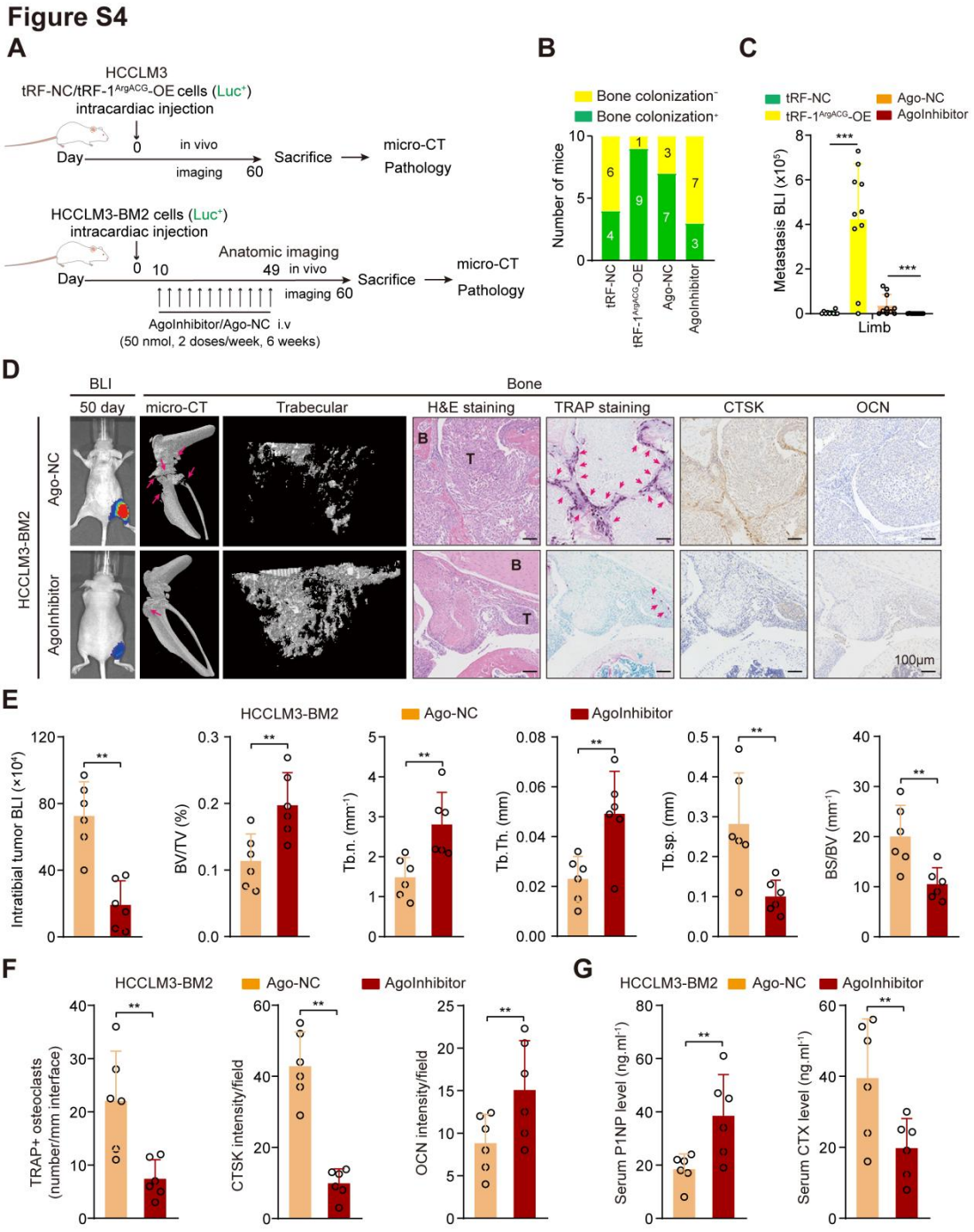


Figure S4. tRF-1^{ArgACG} promotes HCC osteolytic bone metastasis in vivo. (A) Schematic illustration of the experimental design for intracardiac injection-based bone metastasis models using luciferase-labeled HCCLM3 and HCCLM3-BM2 cells, along with the intravenous administration schedule of AgoInhibitor or Ago-NC. HCCLM3 cells with tRF-1^{ArgACG} overexpression or the corresponding control were used to assess the effect of tRF-1^{ArgACG} gain of function, whereas mice inoculated with HCCLM3-BM2 cells received AgoInhibitor or Ago-NC (50 nmol per dose, twice weekly for 6 weeks). (B) Numbers of mice with or without

bone colonization following intracardiac injection of HCCLM3 cells with tRF-1^{ArgACG} overexpression or HCCLM3-BM2 cells treated with AgoInhibitor (n=10 successfully inoculated mice per group). (C) Quantification of endpoint limb metastatic BLI signals in mice with detectable limb metastatic lesions in the indicated groups. (D) Representative BLI images at day 50, micro-CT images, three-dimensional trabecular reconstructions, and H&E, TRAP, CTSK, and OCN staining of tibial tumors from mice intratibially inoculated with HCCLM3-BM2 cells and treated with AgoInhibitor or Ago-NC. B, bone; T, tumor. Scale bars, 100 μm. (E) Quantification of limb metastatic BLI signals and bone structural parameters, including BV/TV, Tb.N, Tb.Th, Tb.Sp, and BS/BV, in the indicated mice. (F) Quantification of TRAP-positive osteoclasts, CTSK, and OCN expression at the bone–tumor interface. (G) Serum levels of P1NP and CTX determined by ELISA in the indicated mice. Data are presented as mean ± SD. $^{**}P < 0.01$; $^{***}P < 0.001$.

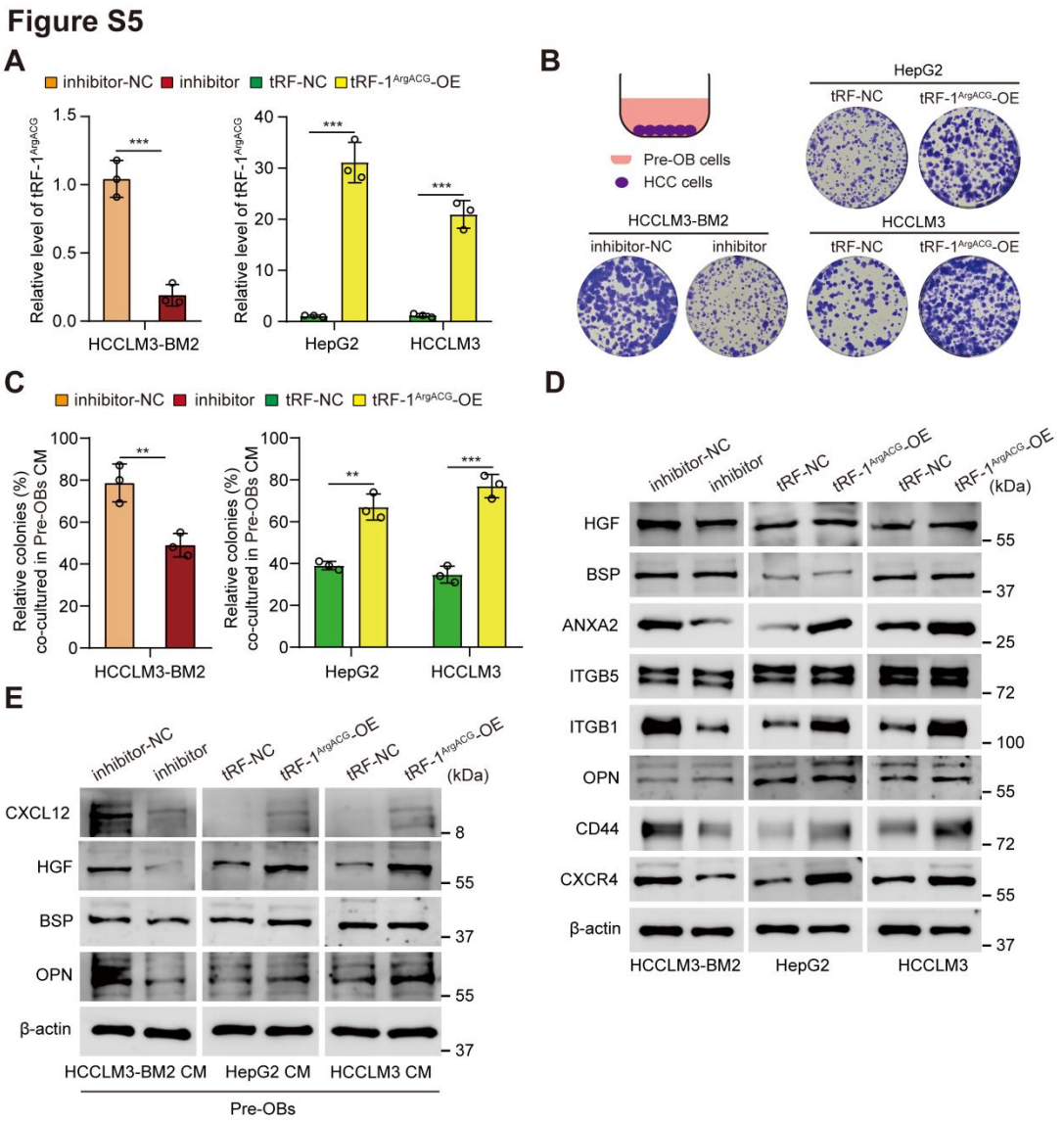


Figure S5. tRF-1^{ArgACG} facilitates HCC cell interactions with the osteoblastic microenvironment. (A) tRF-qPCR analysis of tRF-1^{ArgACG} levels in HCCLM3-BM2 cells following tRF-1^{ArgACG} inhibition and in HepG2 and HCCLM3 cells following tRF-1^{ArgACG} overexpression. (B, C) Representative images (B) and quantification (C) of colony formation by tRF-1^{ArgACG}-modulated HCC cells cultured in Pre-OB-CM. (D) Western blot analysis of HGF, BSP, ANXA2, ITGB5, ITGB1, OPN, CD44, and CXCR4 in HCCLM3-BM2, HepG2, and HCCLM3 cells following tRF-1^{ArgACG} inhibition or overexpression. (E) Western blot analysis of CXCL12, HGF, BSP, and OPN in Pre-OBs exposed to CM from tRF-1^{ArgACG}-modulated HCC cells. Data are presented as mean ± SD of triplicate experiments. *$P < 0.05$; **$P < 0.01$; ***$P < 0.001$.

Figure S6

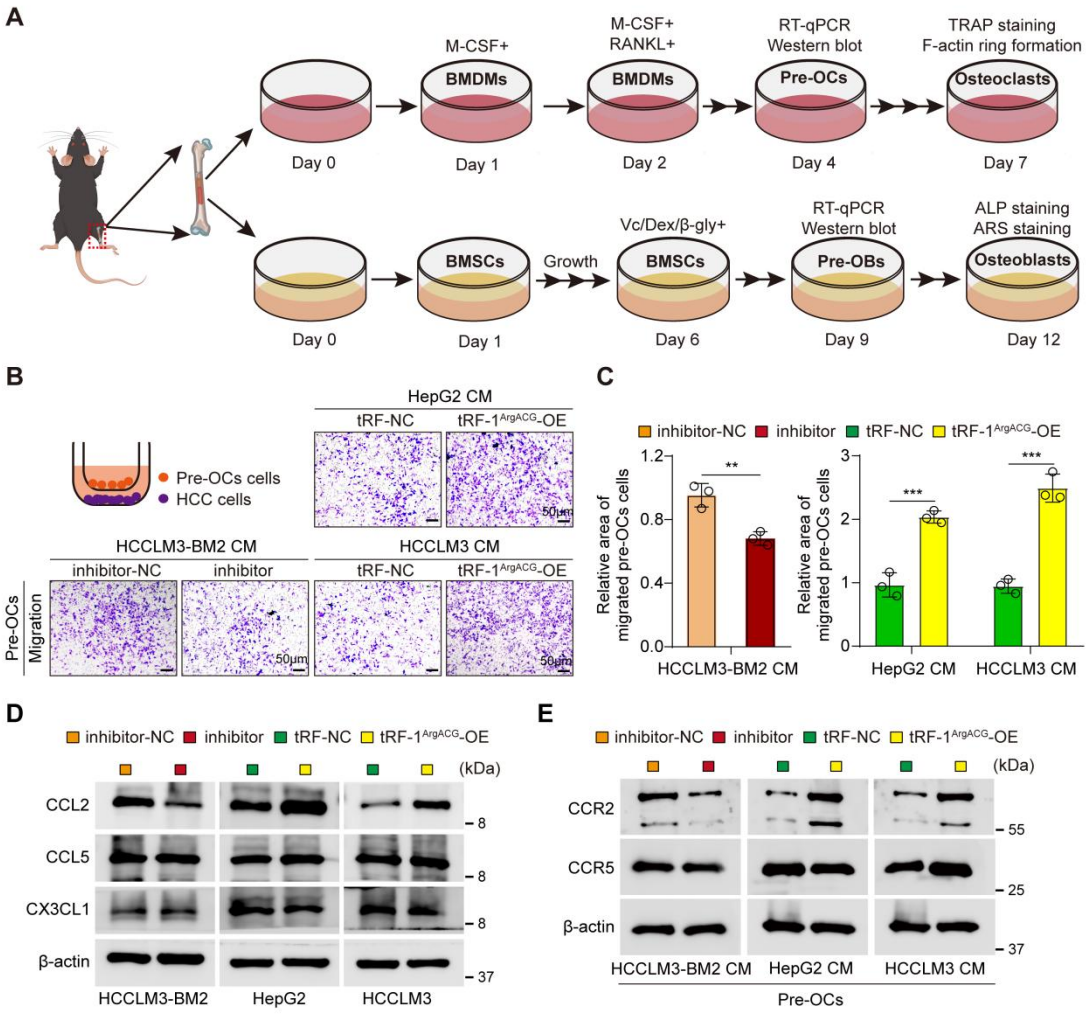


Figure S6. tRF-1^{ArgACG} enhances osteoclastogenesis but restrains osteoblastogenesis *in vitro*. (A) Schematic illustration of the isolation and culture of BMDMs and BMSCs from C57BL/6 mice. (B-C) Representative images (B) and quantification (C) of Transwell assays assessing chemotactic migration of pre-OCs toward HCC cells with tRF-1^{ArgACG} inhibition or overexpression (scale bars = 50 μm). (D) WB was employed to assess the protein expression levels of CCL2, CCL5, and CX3CL1 in HCC cells with tRF-1^{ArgACG} knockdown or overexpression. (E) Western blot analysis of CCR2 and CCR5 in pre-OCs exposed to the indicated HCC CM. Data represent mean ± SD of triplicate experiments. $^{**}P< 0.01$; $^{***}P< 0.001$. ns, not significant.

Figure S7

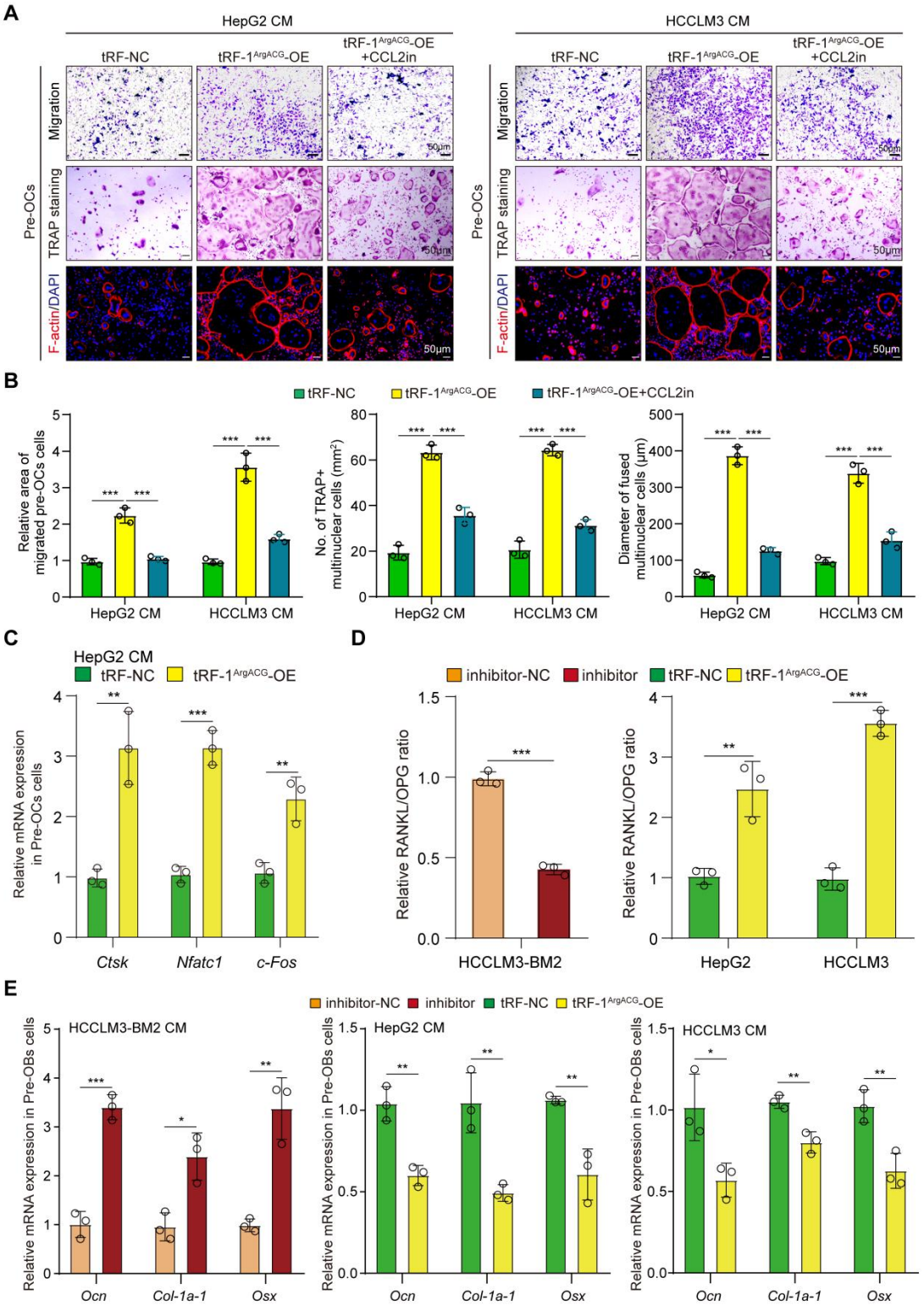


Figure S7. tRF-1^{ArgACG} enhances osteoclastogenesis but restrains osteoblastogenesis *in vitro*. (A-B) HepG2 (left) and HCCLM3 (right) cells were treated with tRF-NC, tRF-1^{ArgACG}, or tRF-1^{ArgACG} in combination with the CCL2 inhibitor Bindarit. Transwell chemotaxis, TRAP staining, and F-actin ring formation assays were performed to evaluate the recruitment and

activation of osteoclast precursors induced by CM from the indicated HCC cells. Representative images (A) and quantitative analysis (B) are shown (scale bars, 50 μm). (C) RT–qPCR analysis was performed to determine the mRNA expression levels of osteoclastogenesis-related markers, including *Ctsk*, *Nfatc1*, and *c-Fos*, in pre-OCs exposed to HepG2-derived CM with or without tRF-1^{ArgACG} overexpression. (D) The relative RANKL/OPG ratio was determined by Western blot analysis in the indicated HCC cells. (E) RT–qPCR analysis was performed to assess the mRNA expression levels of osteogenic markers, including *Ocn*, *Col1a1*, and *Osx*, in pre-OBs exposed to CM from the indicated HCC cells. Data represent mean ± SD of triplicate experiments. **P*< 0.05; ***P*< 0.01; ****P*< 0.001.

Figure S8

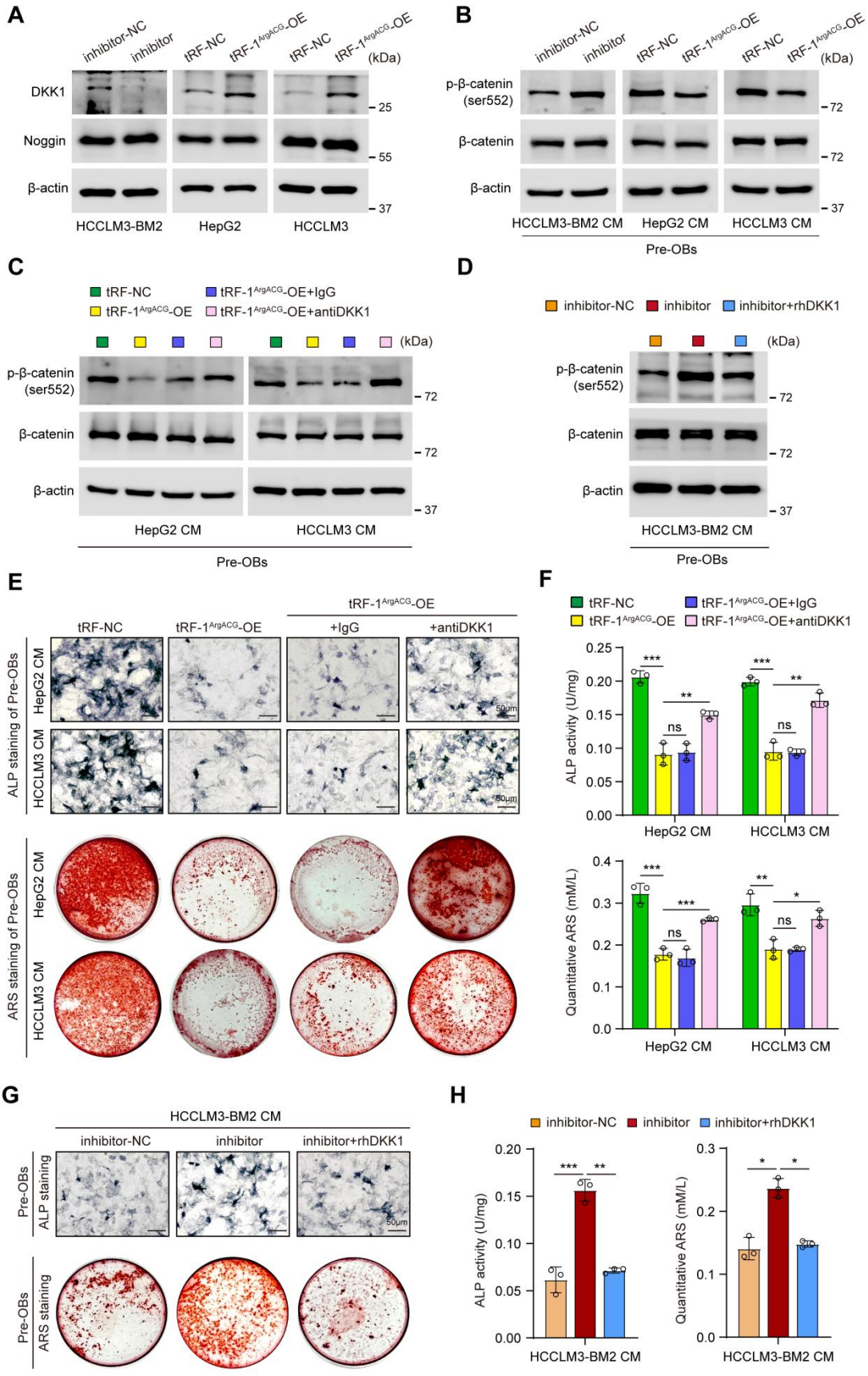


Figure S8. Tumor-derived DKK1 mediates tRF-1^{ArgACG}-induced suppression of

osteoblast differentiation. (A) Western blot analysis of DKK1 and Noggin in HCCLM3-BM2 cells following tRF-1^{ArgACG} inhibition and in HepG2 and HCCLM3 cells following tRF-1^{ArgACG} overexpression. (B) Western blot analysis of phosphorylated β-catenin (Ser552) and total β-catenin in Pre-OBs exposed to CM from tRF-1^{ArgACG}-modulated HCCLM3-BM2, HepG2, or HCCLM3 cells. (C) Western blot analysis of phosphorylated β-catenin (Ser552) and total β-catenin in Pre-OBs exposed to CM from tRF-1^{ArgACG}-overexpressing HepG2 or HCCLM3 cells in the presence of a DKK1-neutralizing antibody or control IgG. (D) Western blot analysis of phosphorylated β-catenin (Ser552) and total β-catenin in Pre-OBs exposed to CM from tRF-1^{ArgACG}-inhibited HCCLM3-BM2 cells with or without recombinant human DKK1 (rhDKK1). (E, F) Representative ALP and ARS staining (E) and quantification of ALP activity and mineralization (F) in Pre-OBs exposed to CM from tRF-1^{ArgACG}-overexpressing HepG2 or HCCLM3 cells in the presence of a DKK1-neutralizing antibody or control IgG. (G, H) Representative ALP and ARS staining (G) and quantification of ALP activity and mineralization (H) in Pre-OBs exposed to CM from tRF-1^{ArgACG}-inhibited HCCLM3-BM2 cells with or without rhDKK1. Data are presented as mean ± SD of triplicate experiments. *P < 0.05; **P < 0.01; ***P < 0.001; ns, not significant.

Figure S9

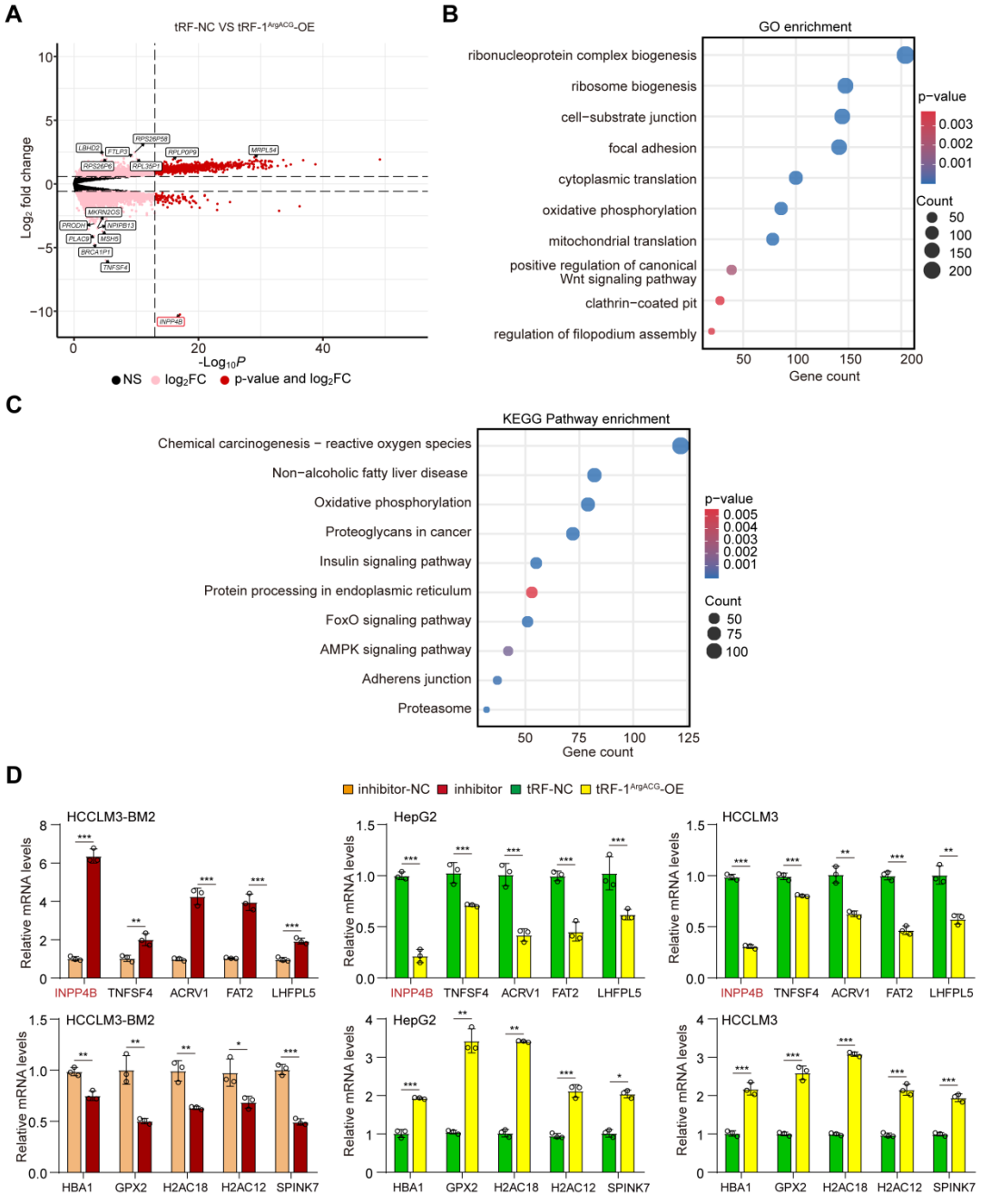


Figure S9. Identification of INPP4B from RNA-seq. (A) Volcano plot illustrating the upregulated and downregulated DEGs in HCCLM3/tRF-1^{ArgACG} compared to HCCLM3/tRF-NC cells. (B-C) GO (B) and KEGG (C) enrichment analyses of the differentially expressed genes identified by RNA-seq. (D) RT-qPCR assays assessed the mRNA levels of top 5 downregulated and 5 upregulated genes in HCC cells with tRF-1^{ArgACG} inhibition or overexpression. Data represent mean ± SD of triplicate experiments. *P< 0.05; **P< 0.01; ***P< 0.001. ns, not significant.

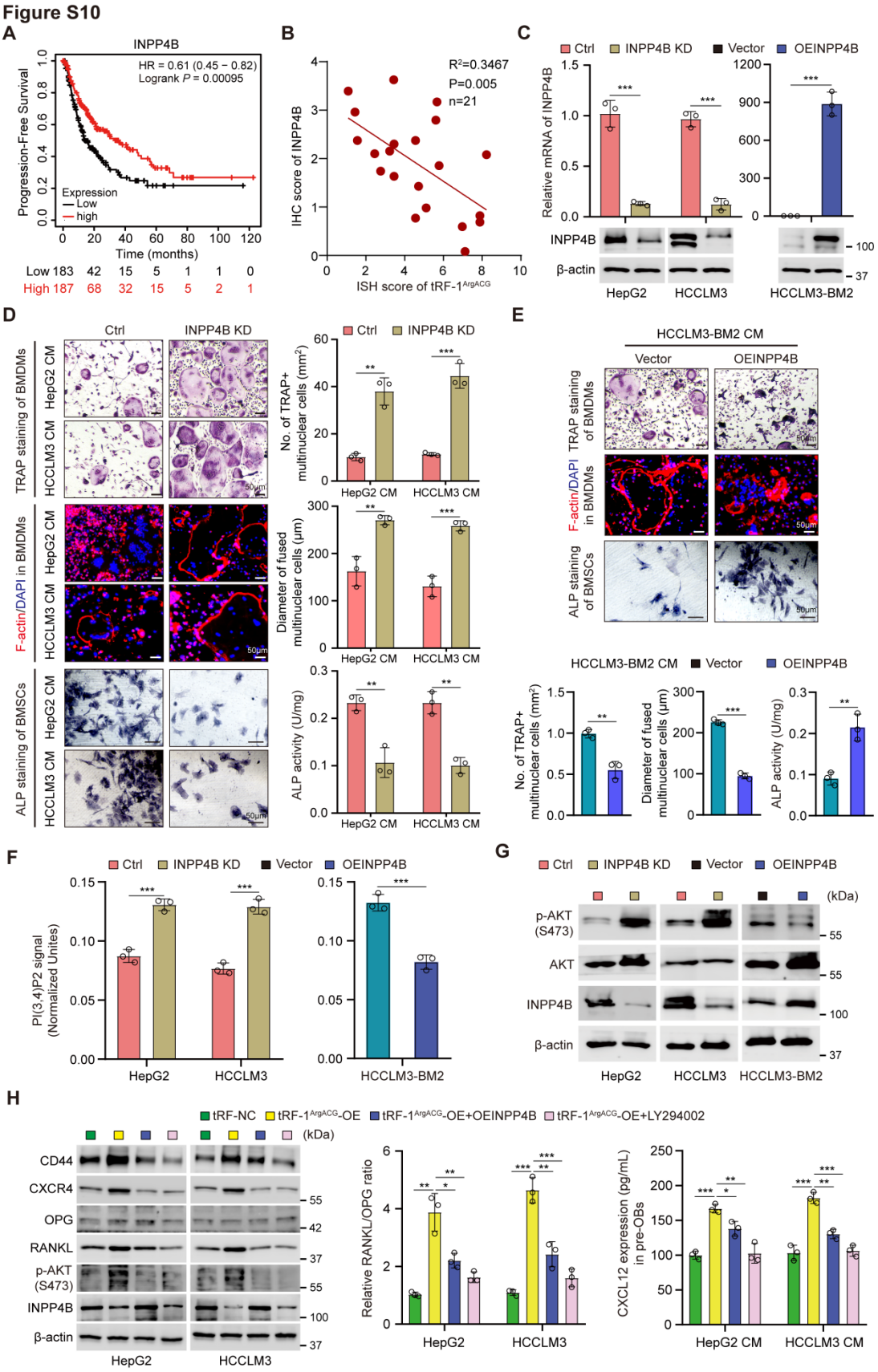


Figure S10. tRF-1^{ArgACG}-induced INPP4B suppression and PI3K/AKT activation disrupt bone homeostasis in HCC. (A) Kaplan-Meier analysis of PFS in HCC patients stratified by

high or low INPP4B expression obtained from TCGA database (HR = 0.61, 95% CI: 0.45-0.82, *P* = 0.00095; log-rank test). (B) Pearson correlation analysis of INPP4B IHC score with tRF-1^{ArgACG} ISH score in 21 bone-metastatic lesions (n=21, R^2=0.3467, *P*=0.005). (C) RT-qPCR and Western blot assays were used to assess the mRNA and protein levels of INPP4B in HCC cells with INPP4B knockdown or overexpression. (D) TRAP staining, F-actin ring formation and ALP staining assays were performed to evaluate osteoclastogenesis and osteoblastogenesis differences in the presence of CM from HepG2 and HCCLM3 cells with INPP4B silencing. Representative images (left) and quantification (right) are shown (Scale bars, 50 μm). (E) TRAP staining, F-actin ring formation and ALP staining assays were performed to evaluate osteoclastogenesis and osteoblastogenesis differences in the presence of CM from HCCLM3-BM2 cells with INPP4B overexpression. Representative images (top) and quantification (bottom) are shown (Scale bars, 50 μm). (F) ELISA assays were used to determine the PI(3,4)P2 levels in the indicated HCC cells. (G) Western blot analysis of INPP4B, total AKT, and phosphorylated AKT (Ser473) in the indicated HCC cells as above. (H) HepG2 and HCCLM3 cells were treated with tRF-NC, tRF-1^{ArgACG}, tRF-1^{ArgACG} combined with INPP4B restoration or LY294002 co-treatment. Western blot analysis of INPP4B, phosphorylated AKT (Ser473), RANKL, OPG, CD44 and CXCR4 in the indicated HCC cells as above (left). Relative RANKL/OPG ratios were assessed according to Western blot data in the indicated HCC cells (middle). Secreted CXCL12 levels were tested by ELISA assays in pre-OBs treated with CM from the indicated HCC cells (right). Data represent mean ± SD of triplicate experiments. **P*< 0.05; ***P*< 0.01; ****P*< 0.001.

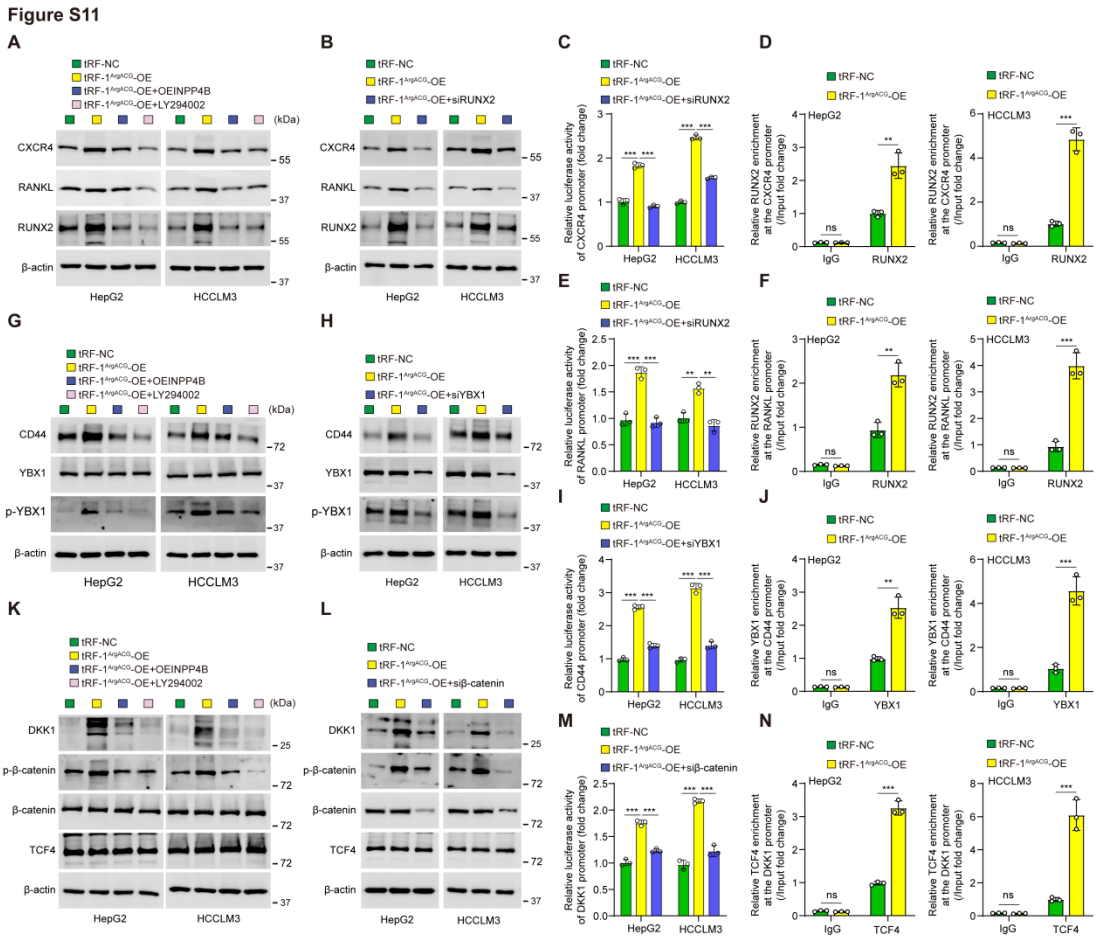


Figure S11. PI3K/AKT activation regulates CXCR4, RANKL, CD44, and DKK1 through distinct downstream transcriptional pathways. (A, B) Western blot analysis of RUNX2, CXCR4, and RANKL following tRF-1^{ArgACG} overexpression with INPP4B restoration, LY294002 treatment (A), or RUNX2 silencing (B). (C–F) CXCR4 and RANKL promoter luciferase assays following RUNX2 silencing (C, E) and ChIP-qPCR analysis of RUNX2 enrichment at the CXCR4 and RANKL promoters (D, F). (G, H) Western blot analysis of YBX1, phosphorylated YBX1, and CD44 following tRF-1^{ArgACG} overexpression with INPP4B restoration, LY294002 treatment (G), or YBX1 silencing (H). (I, J) CD44 promoter luciferase assay following YBX1 silencing (I) and ChIP-qPCR analysis of YBX1 enrichment at the CD44 promoter (J). (K, L) Western blot analysis of DKK1, phosphorylated β-catenin, total β-catenin, and TCF4 following tRF-1^{ArgACG} overexpression with INPP4B restoration, LY294002 treatment (K), or β-catenin silencing (L). (M, N) DKK1 promoter luciferase assay following β-catenin silencing (M) and ChIP-qPCR analysis of TCF4 enrichment at the DKK1 promoter (N). Data are presented as mean ± SD of triplicate

experiments. *$P < 0.05$; **$P < 0.01$; ***$P < 0.001$; ns, not significant.

Figure S12

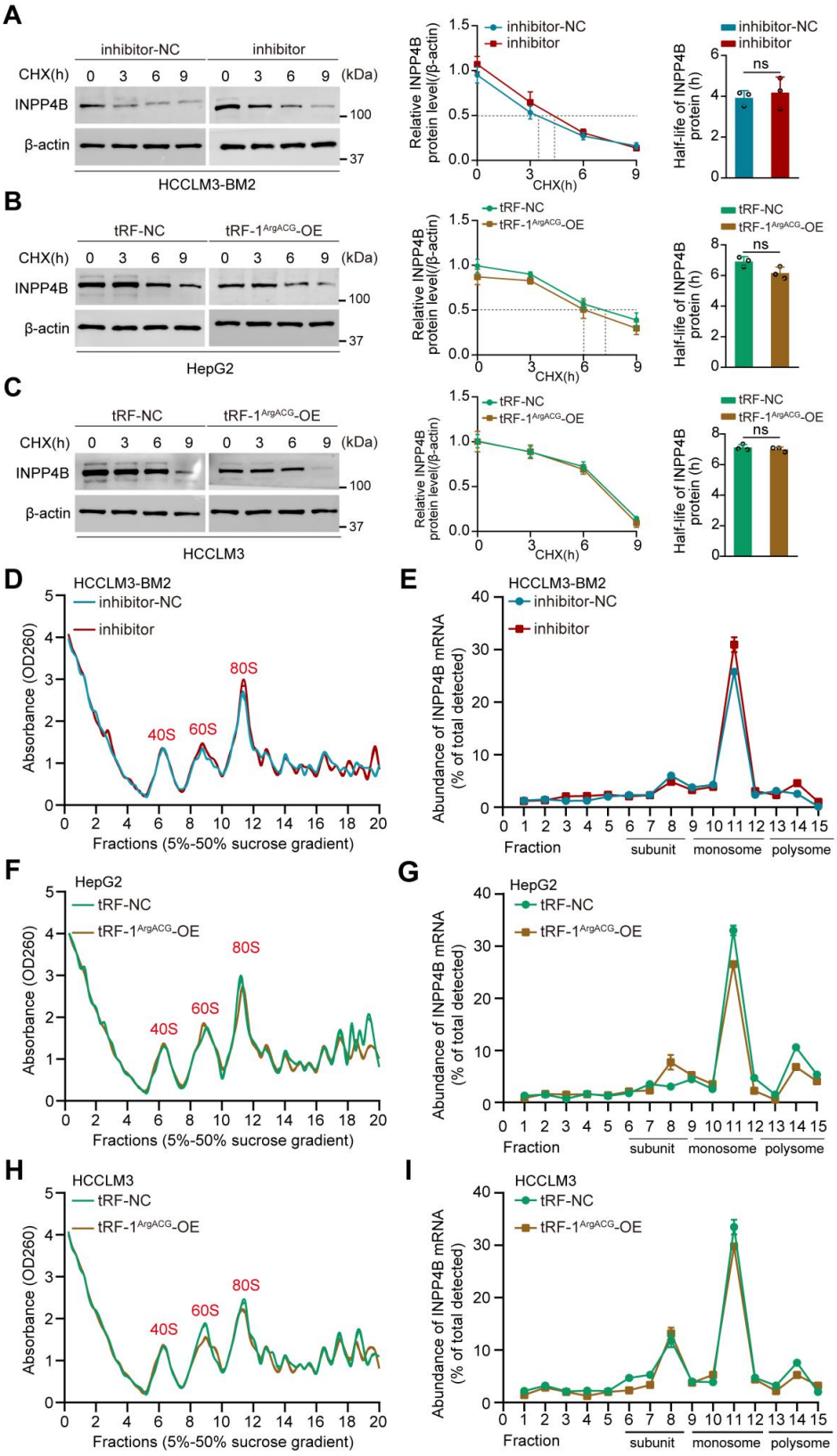


Figure S12. The effect of tRF-1^{ArgACG} on INPP4B protein stability and translational activity in HCC Cells. (A-C) Cycloheximide (CHX) chase assays were performed to evaluate the stability of INPP4B protein in HCC cells under different conditions. HCCLM3-BM2 cells treated with inhibitor or inhibitor-NC (A), HepG2 cells (B), and HCCLM3 cells (C) with tRF-1^{ArgACG} overexpression or control were exposed to CHX and collected at the indicated time points. Immunoblotting was performed to detect INPP4B protein levels. The left panels show representative Western blot images, and the middle panels display quantification of relative INPP4B protein levels normalized to β-actin. The right panels present the calculated half-life of INPP4B protein based on densitometric analysis using ImageJ software. (D–I) Polysome profiling analysis was conducted to assess the translational status of INPP4B mRNA in HCC cells following tRF-1^{ArgACG} modulation. Sucrose gradient fractionation (5–50%) was performed, and absorbance at 260 nm (OD260) was recorded to visualize ribosomal subunits (40S, 60S) and polysome distribution (D, F, H). The distribution of INPP4B mRNA across fractions was determined by RT-qPCR and presented as the percentage of total detected mRNA (E, G, I). Data represent mean ± SD of triplicate experiments. ns, not significant.

Figure S13

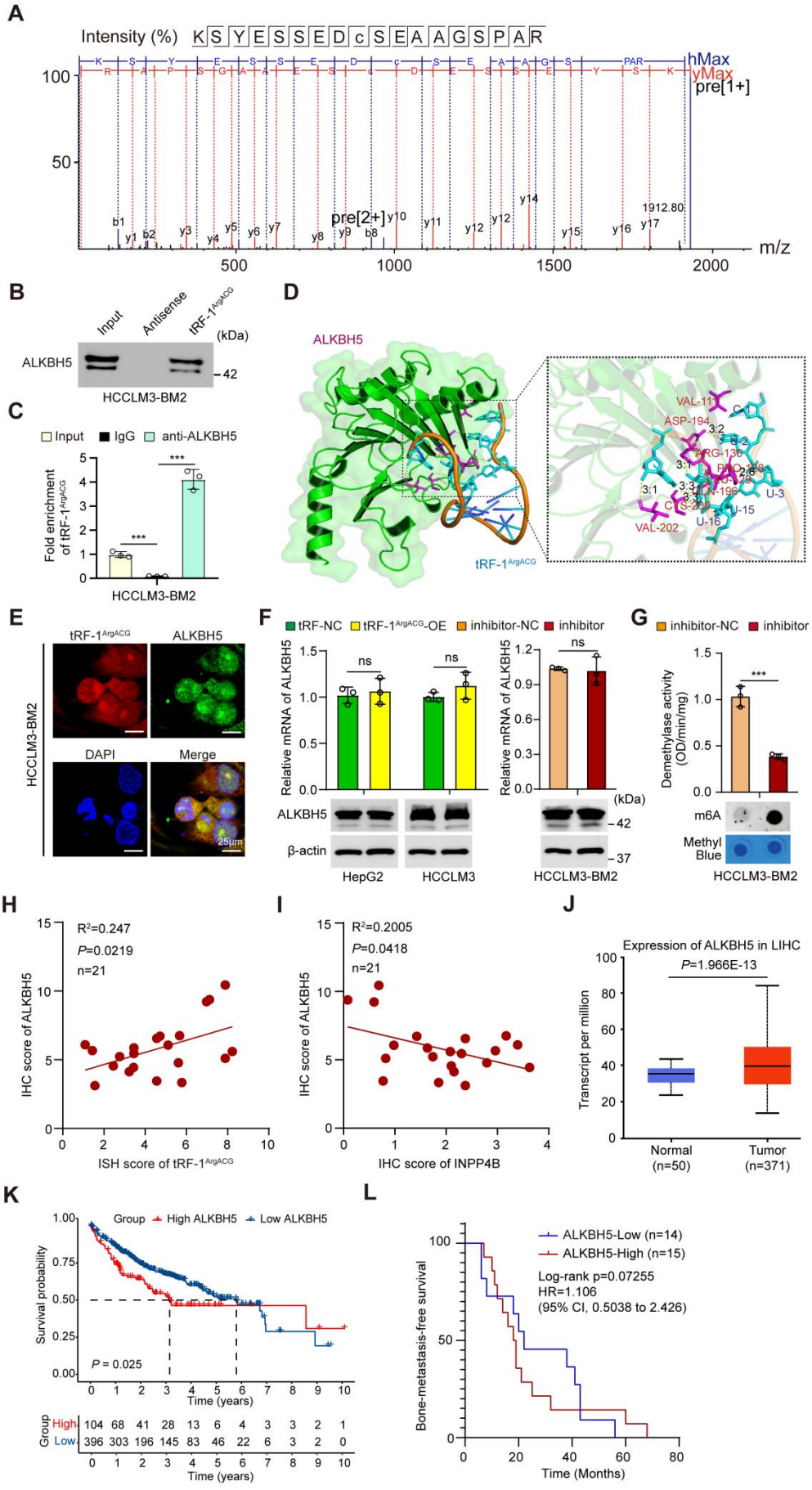

A
Intensity (%)
K S Y E S S E D c S E A A G S P A R
hMax
yMax
pre[1+]
pre[2+]
1912.80
m/z
B
Input
Antisense
tRF-1ArgACG
(kDa)
ALKBH5
42
HCCLM3-BM2
C
Input
IgG
anti-ALKBH5
Fold enrichment of tRF-1ArgACG
HCCLM3-BM2
D
ALKBH5
tRF-1ArgACG
VAL-111
ASP-194
ARG-130
VAL-202
U-3
U-15
U-16
E
tRF-1ArgACG
ALKBH5
DAPI
Merge
HCCLM3-BM2
25μm
F
tRF-NC
tRF-1ArgACG-OE
inhibitor-NC
inhibitor
Relative mRNA of ALKBH5
ns
ALKBH5
β-actin
(kDa)
42
37
HepG2
HCCLM3
HCCLM3-BM2
G
inhibitor-NC
inhibitor
Demethylase activity (OD/min/mg)
m6A
Methyl Blue
HCCLM3-BM2
H
R²=0.247
P=0.0219
n=21
IHC score of ALKBH5
ISH score of tRF-1ArgACG
I
R²=0.2005
P=0.0418
n=21
IHC score of ALKBH5
IHC score of INPP4B
J
Expression of ALKBH5 in LIHC
P=1.966E-13
Transcript per million
Normal (n=50)
Tumor (n=371)
K
Group
High ALKBH5
Low ALKBH5
Survival probability
P = 0.025
Time (years)
High 104 68 41 28 13 6 4 3 3 2 1
Low 396 303 196 145 83 46 22 6 3 2 0
L
ALKBH5-Low (n=14)
ALKBH5-High (n=15)
Log-rank p=0.07255
HR=1.106
(95% CI, 0.5038 to 2.426)
Bone-metastasis-free survival
Time (Months)

Figure S13. tRF-1^{ArgACG} suppresses INPP4B through enhancing ALKBH5 demethylase activity. (A) MS/MS spectrum of a unique peptide derived from ALKBH5. (B) Western blot analysis showing specific enrichment of ALKBH5 in tRF-1^{ArgACG} RNA pull-down products from HCCLM3-BM2 cell lysates. Antisense RNA was used as a negative control. (C) RIP assays were performed using anti-ALKBH5 or control IgG antibodies in HCCLM3-BM2 cells. tRF-qPCR assays revealed significant enrichment of tRF-1^{ArgACG} in ALKBH5-associated complexes compared to IgG controls. (D) Predicted 3D structure of the ALKBH5–tRF-1^{ArgACG} complex based on molecular docking analysis, highlighting the predicted interacting residues and nucleotides. (E) Subcellular co-localization of tRF-1^{ArgACG} and ALKBH5 in HCCLM3-BM2 cells visualized by combined FISH and IF staining. Nuclei were counterstained with DAPI (scale bar, 25 μm). (F) RT-qPCR and Western blot assays were used to examine ALKBH5 mRNA and protein levels in the indicated HCC cells following tRF-1^{ArgACG} inhibition or overexpression. (G) Demethylase activity assays and m6A dot blot were performed to assess ALKBH5 demethylase activity and m6A levels in HCCLM3-BM2 cells following tRF-1^{ArgACG} inhibition. Methylene blue staining was used as a loading control. (H) Pearson correlation analysis between ALKBH5 IHC scores and tRF-1^{ArgACG} ISH scores in bone-metastatic lesions (n = 21, R^2 = 0.247, P = 0.0219). (I) Pearson correlation analysis between ALKBH5 and INPP4B IHC scores in bone-metastatic lesions (n = 21, R^2 = 0.2005, P = 0.0418). (J) ALKBH5 expression in HCC tissues (n = 371) and normal liver tissues (n = 50) from the TCGA dataset. (K) Kaplan-Meier analysis of OS in HCC patients stratified by high or low ALKBH5 expression in the combined public datasets (n = 500; P = 0.025; log-rank test). (L) Kaplan-Meier analysis of BMFS in HCC patients with high or low ALKBH5 expression levels in our clinical cohort (n = 29; median staining score of 5.708 was used as the cut-off; HR = 1.106, 95% CI: 0.5038–2.426, P = 0.07255; log-rank test). Data represent mean ± SD. ***$P < 0.001$. ns, not significant.

Figure S14

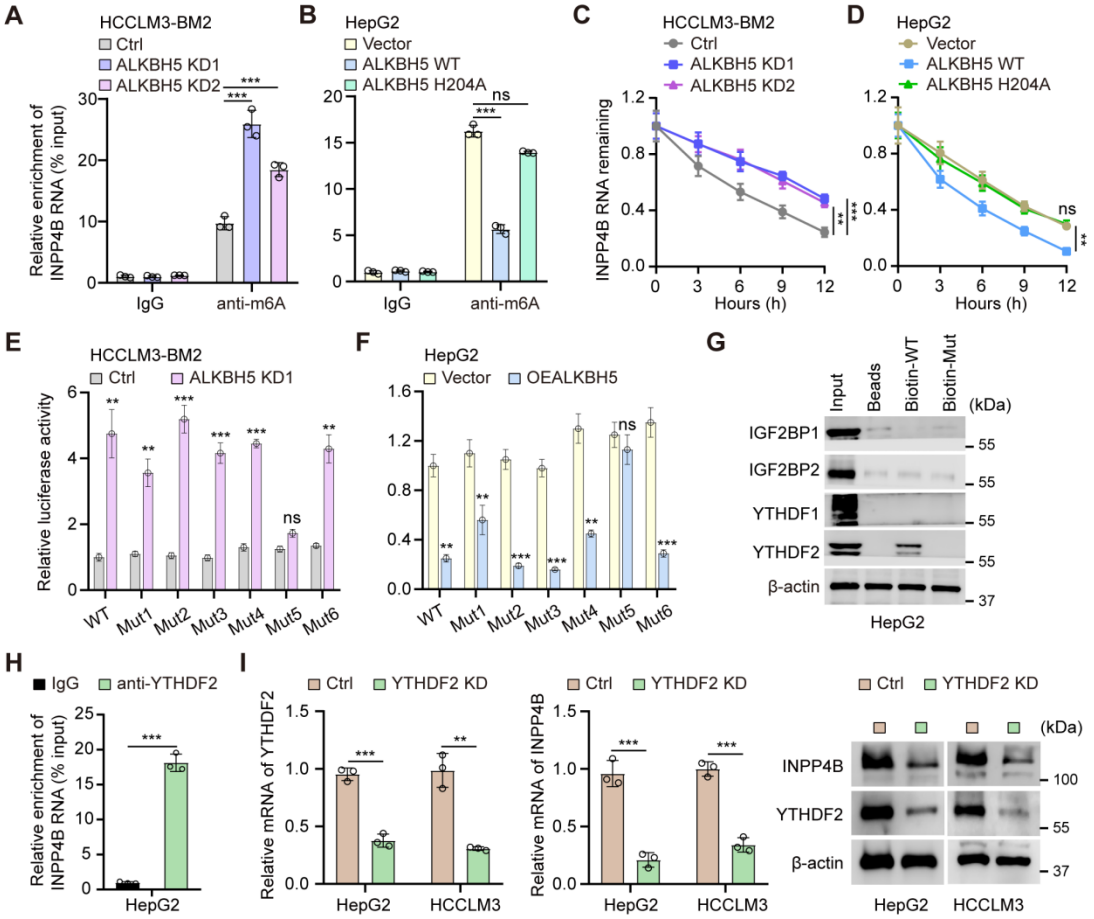


Figure S14. ALKBH5 destabilizes INPP4B mRNA in an m6A-YTHDF2-dependent manner. (A-B) MeRIP-qPCR assays determined the m6A modification level of INPP4B mRNA in HCCLM3-BM2 cells after ALKBH5 inhibition (A) and in HepG2 cells expressing ALKBH5-WT or ALKBH5-MUT (B). (C-D) INPP4B mRNA stability was assessed by RT-qPCR in HCCLM3-BM2 cells with ALKBH5 knockdown (C) and in HepG2 cells transfected with ALKBH5-WT or ALKBH5-MUT (D) following actinomycin D treatment at the indicated time points. (E) Relative luciferase activity (Firefly/Renilla) in HCCLM3-BM2 cells co-treated with Ctrl/ALKBH5 knockdown and INPP4B-WT or INPP4B-Mut reporters. (F) Relative luciferase activity in HepG2 cells co-transfected with Vector-NC/ALKBH5 plasmids and INPP4B-WT or INPP4B-Mut reporters. (G) RNA pull-down assays were performed using biotin-labeled wild-type or m6A site-mutated INPP4B RNA probes in HepG2 cell lysates, followed by Western blot analysis of IGF2BP1, IGF2BP2, YTHDF1, and YTHDF2. Input and beads-only samples served as controls. (H) RIP assays were performed using anti-YTHDF2 or control IgG antibodies in HepG2 cells. RT-qPCR assays revealed

significant enrichment of INPP4B in YTHDF2-associated complexes compared to IgG controls. (I) RT-qPCR and Western blot assays of YTHDF2 knockdown efficiency and its effect on INPP4B expression in HepG2 and HCCLM3 cells. Data represent mean ± SD of triplicate experiments. ***P*< 0.01; ****P*< 0.001. ns, not significant.

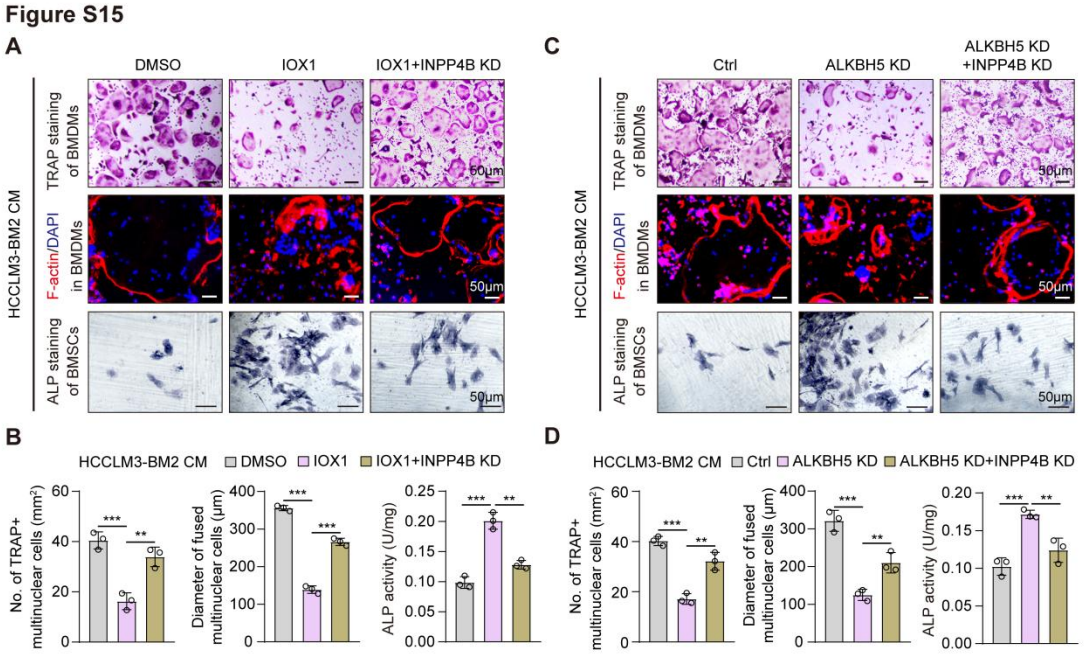


Figure S15. ALKBH5 inhibition attenuates the disruption of bone homeostasis that could be reversed by INPP4B knockdown. (A-B) HCCLM3-BM2 cells were treated with DMSO, IOX1, and IOX1 combined with INPP4B silencing. TRAP staining, F-actin ring formation and ALP staining assays were performed to evaluate osteoclastogenesis and osteoblastogenesis differences in the presence of CM from HCCLM3-BM2 cells with different regimens. Representative images (A) and quantification (B) are shown (Scale bars, 50 μm). (C-D) HCCLM3-BM2 cells were treated with negative control, ALKBH5 knockdown, and ALKBH5 knockdown combined with INPP4B silencing. TRAP staining, F-actin ring formation and ALP staining assays were performed to evaluate osteoclastogenesis and osteoblastogenesis differences in the presence of CM from HCCLM3-BM2 cells with different regimens. Representative images (C) and quantification (D) are shown (Scale bars, 50 μm). Data represent mean ± SD of triplicate experiments. ***P*< 0.01; ****P*< 0.001.

Figure S16

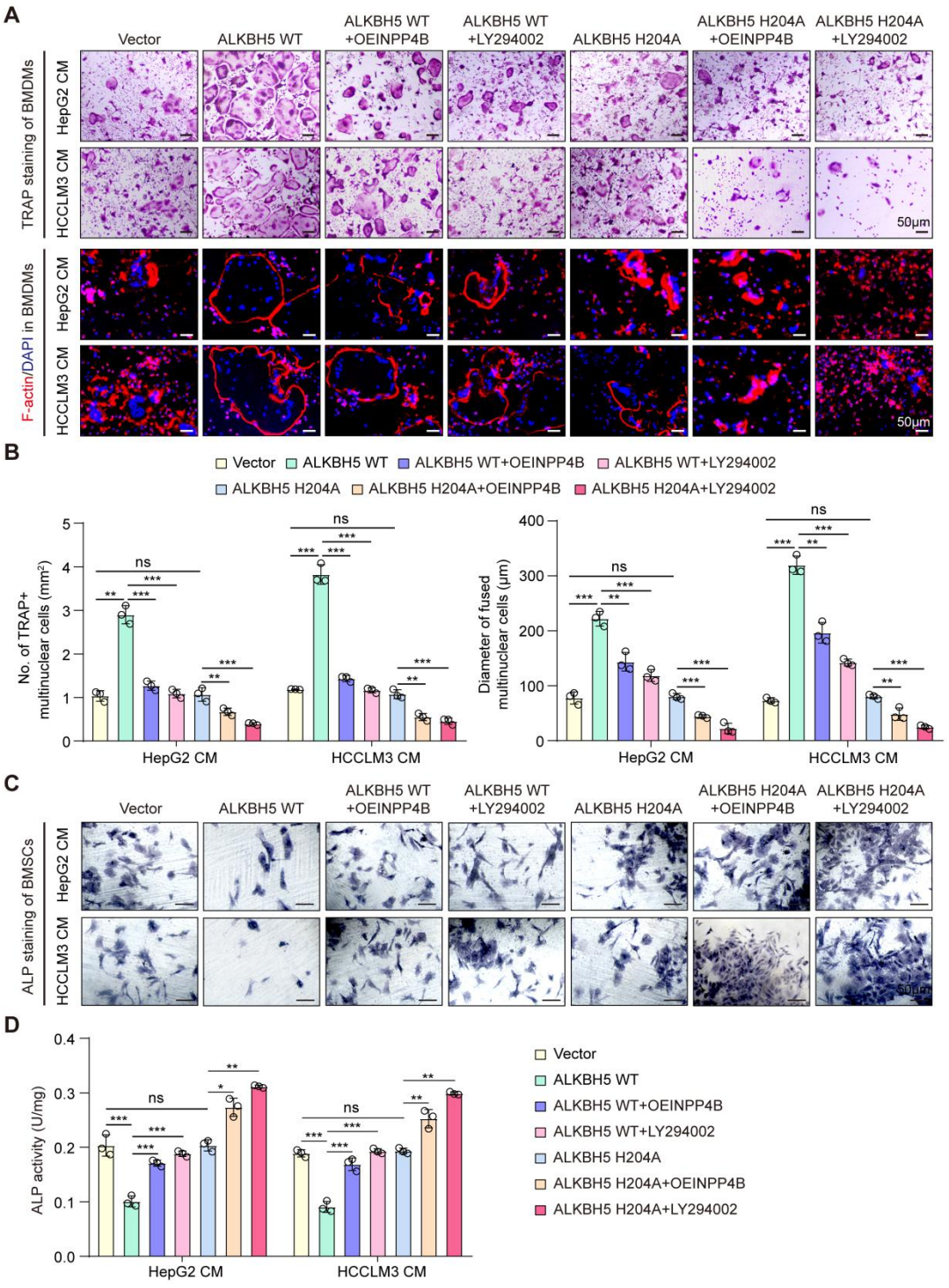


Figure S16. ALKBH5 disrupts bone homeostasis by suppressing INPP4B *via* m⁶A demethylation. (A-B) HepG2 and HCCLM3 cells were treated with Vector-NC, overexpression of ALKBH5 WT, overexpression of ALKBH5 WT combined with INPP4B restoration, overexpression of ALKBH5 WT combined with LY294002 treatment, overexpression of ALKBH5 H204A mutant, overexpression of ALKBH5 H204A mutant

combined with INPP4B restoration, and overexpression of ALKBH5 H204A mutant combined with LY294002 co-treatment. TRAP staining and F-actin ring formation were performed to evaluate osteoclastogenesis in the presence of CM from HepG2 or HCCLM3 cells with different regimens. Representative images (A) and quantification (B) are shown (Scale bars, 50 μm). (C-D) ALP staining assays were used to assess osteoblastogenesis in the presence of CM from the indicated HCC cells as above. Representative images (C) and quantification (D) are shown (Scale bars, 50 μm). Data represent mean ± SD of triplicate experiments. **P*< 0.05; ***P*< 0.01; ****P*< 0.001. ns, not significant.

Figure S17

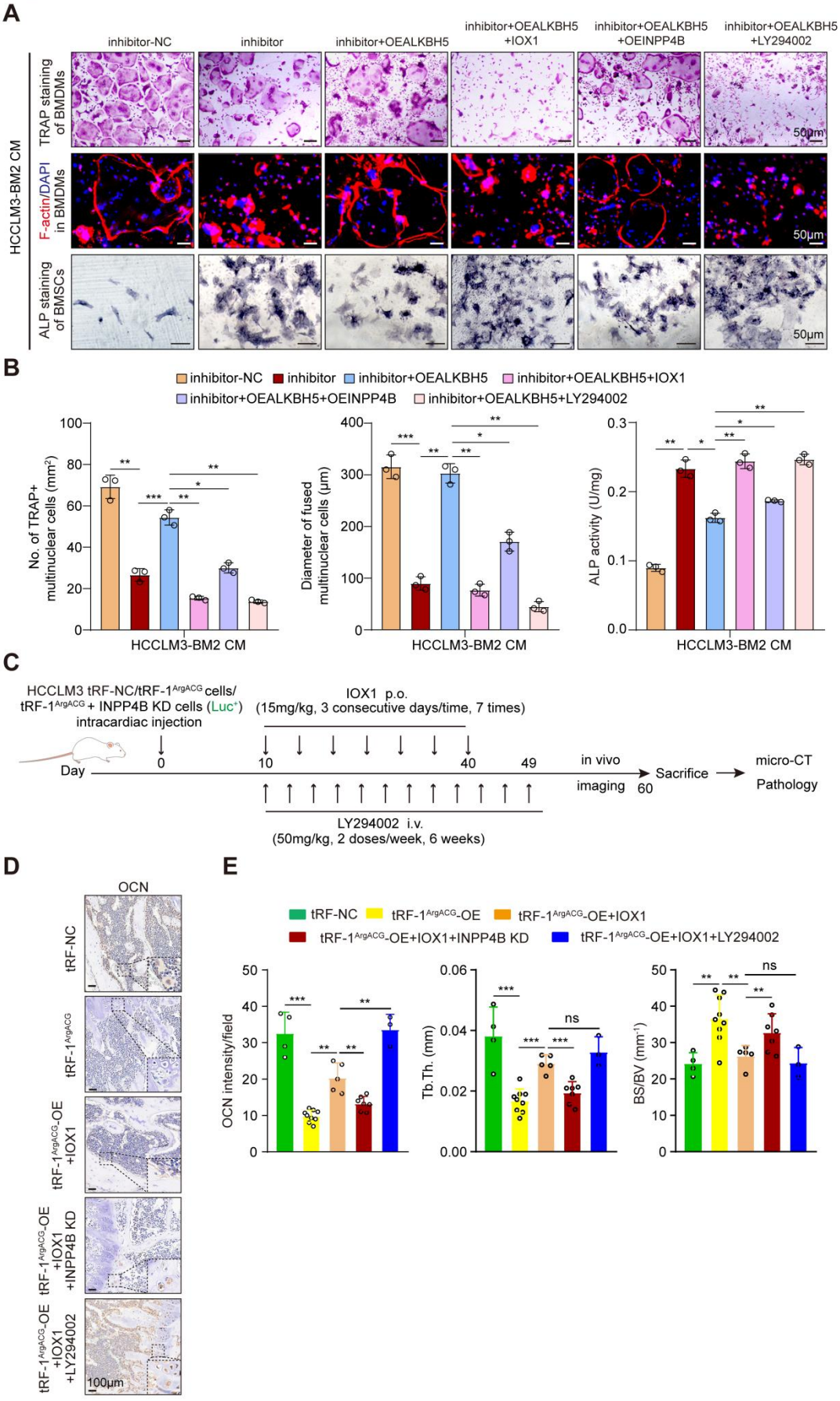

A
inhibitor-NC
inhibitor
inhibitor+OEALKBH5
inhibitor+OEALKBH5 +IOX1
inhibitor+OEALKBH5 +OEINPP4B
inhibitor+OEALKBH5 +LY294002
HCCLM3-BM2 CM
TRAP staining of BMDMs
F-actin/DAPI in BMDMs
ALP staining of BMSCs
50μm
B
inhibitor-NC
inhibitor
inhibitor+OEALKBH5
inhibitor+OEALKBH5+IOX1
inhibitor+OEALKBH5+OEINPP4B
inhibitor+OEALKBH5+LY294002
No. of TRAP+ multinuclear cells (mm²)
Diameter of fused multinuclear cells (μm)
ALP activity (U/mg)
HCCLM3-BM2 CM
C
HCCLM3 tRF-NC/tRF-1ArgACG cells/ tRF-1ArgACG + INPP4B KD cells (Luc+) intracardiac injection
IOX1 p.o. (15mg/kg, 3 consecutive days/time, 7 times)
Day
0
10
40
49
in vivo imaging
Sacrifice
60
micro-CT
Pathology
LY294002 i.v. (50mg/kg, 2 doses/week, 6 weeks)
D
OCN
tRF-NC
tRF-1ArgACG
tRF-1ArgACG-OE +IOX1
tRF-1ArgACG-OE +IOX1 +INPP4B KD
tRF-1ArgACG-OE +IOX1 +LY294002
100μm
E
tRF-NC
tRF-1ArgACG-OE
tRF-1ArgACG-OE+IOX1
tRF-1ArgACG-OE+IOX1+INPP4B KD
tRF-1ArgACG-OE+IOX1+LY294002
OCN intensity/field
Tb.Th. (mm)
BS/BV (mm⁻¹)
ns

Figure S17. tRF-1^{ArgACG} disrupts bone homeostasis through modulating the ALKBH5/INPP4B/PI3K/AKT axis in HCC. (A–B) TRAP staining, F-actin ring formation and ALP staining assays were performed to evaluate osteoclastogenesis and osteoblastogenesis in the presence of CM from HCCLM3-BM2 cells subjected to the indicated treatments. Representative images (A) and quantification (B) are shown (scale bars, 50 μm). (C) Schematic illustration of the experimental design for the intracardiac bone metastasis model using HCCLM3-derived cells with the indicated genetic manipulations. Mice were treated with IOX1 (15 mg/kg, p.o., 3 consecutive days per cycle for 7 cycles) and/or LY294002 (50 mg/kg, i.v., twice per week for 6 weeks), followed by *in vivo* imaging and endpoint analyses (n = 10 successfully injected mice per group). (D) Representative OCN staining of bone lesions from the indicated mice (scale bars, 100 μm). (E) Quantification of OCN staining, Tb.Th, and BS/BV in the indicated groups. Data represent mean ± SD. **P* < 0.05; ***P* < 0.01; ****P* < 0.001. ns, not significant.

Figure S18

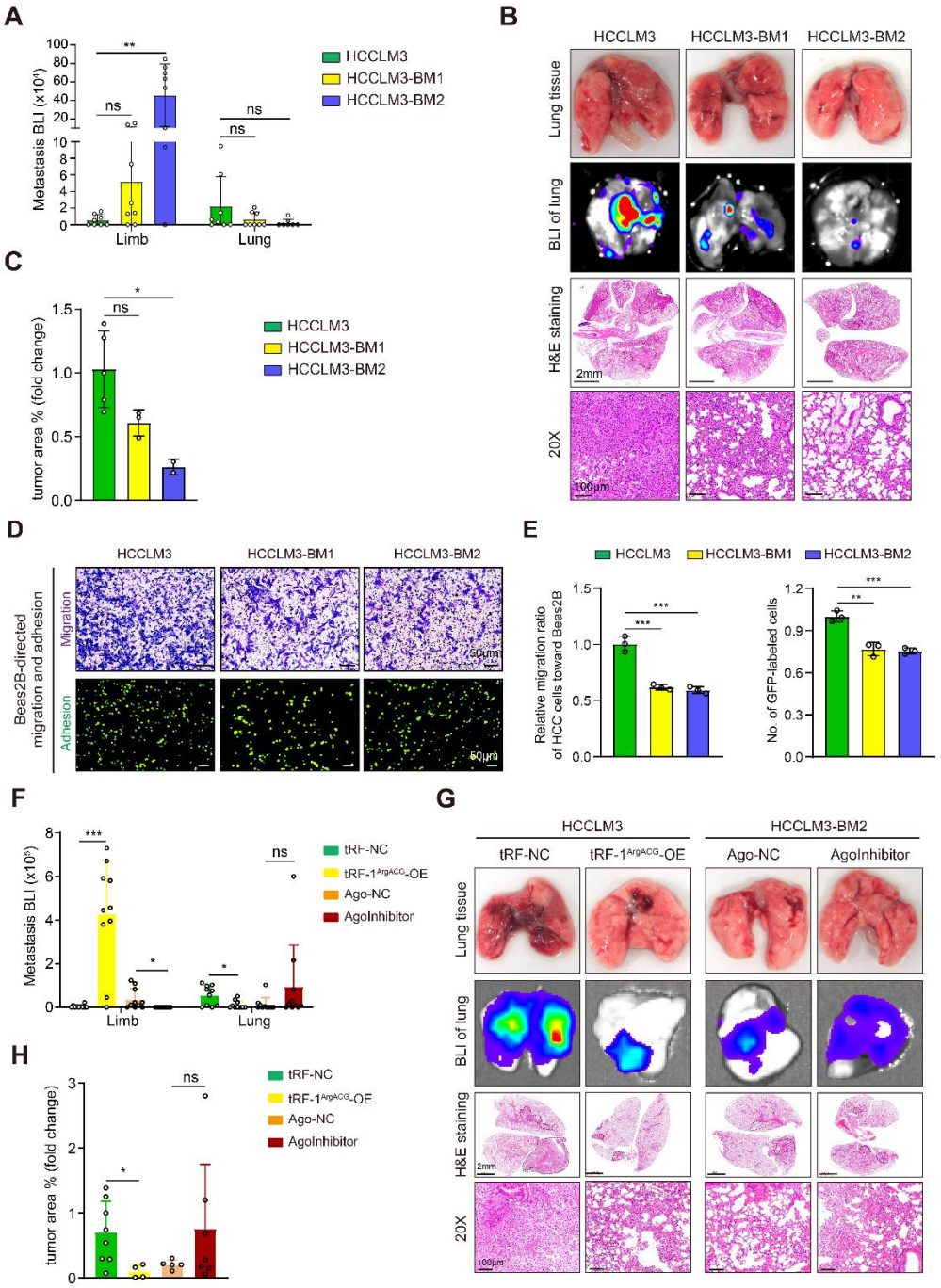


Figure S18. Assessment of pulmonary metastatic involvement during bone-metastatic selection and tRF-1^{ArgACG} modulation. (A) Quantification of metastatic BLI signals in the limbs and lungs of mice inoculated with HCCLM3, HCCLM3-BM1, or HCCLM3-BM2 cells. (B) Representative gross lung images, ex vivo lung BLI, and H&E staining of lung tissues from the indicated groups. Scale bars, 2 mm and 100 μm. (C) Quantification of pulmonary tumor area in the indicated groups. (D–E) Representative images (D) and quantification (E) of

Beas2B-directed migration and adhesion of HCCLM3, HCCLM3-BM1, and HCCLM3-BM2 cells. Scale bars, 50 μm. (F) Quantification of metastatic BLI signals in the limbs and lungs of mice following tRF-1^{ArgACG} overexpression or inhibition. (G) Representative gross lung images, ex vivo lung BLI, and H&E staining of lung tissues from the indicated groups. Scale bars, 2 mm and 100 μm. (H) Quantification of pulmonary tumor area in the indicated groups. Data are presented as mean ± SD. *$P < 0.05$; **$P < 0.01$; ***$P < 0.001$. ns, not significant.

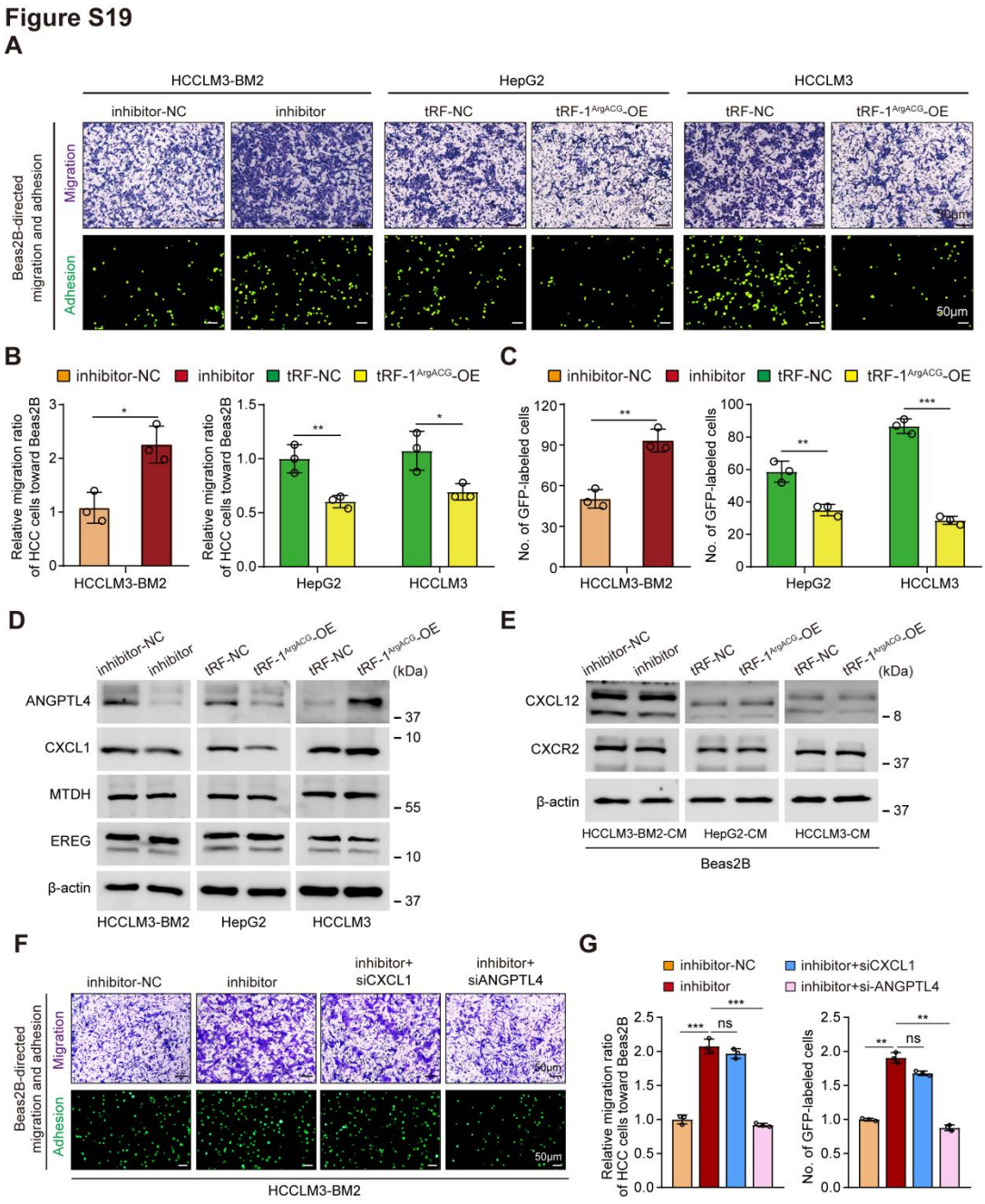


Figure S19. Effects of tRF-1^{ArgACG} modulation on lung-associated HCC cell phenotypes. (A–C) Representative images (A) and quantification of Beas2B-directed migration (B) and

adhesion (C) of HCCLM3-BM2, HepG2, and HCCLM3 cells following tRF-1^{ArgACG} inhibition or overexpression. Scale bars, 50 μm. (D-E) Western blot analysis of ANGPTL4, CXCL1, MTDH, and EREG in HCC cells (D), and CXCL12 and CXCR2 in Beas2B cells (E) exposed to CM from the indicated HCC cells. (F-G) Representative images (F) and quantification (G) of Beas2B-directed migration and adhesion of HCCLM3-BM2 cells following tRF-1^{ArgACG} inhibition with or without CXCL1 or ANGPTL4 silencing. Scale bars, 50 μm. Data are presented as mean ± SD. *P < 0.05; **P < 0.01; ***P < 0.001. ns, not significant.

Supplementary materials and methods

Cell lines and culture: Human HCC cell lines (HepG2, Huh7, H7402 and HCCLM3), human embryonic kidney cells (293T) and immortalized lung epithelial Beas-2B cells were obtained from the ATCC. All cells were cultured in Dulbecco's modified Eagle's medium (DMEM; Cellmax, CGM101.05, Beijing, China) supplemented with 10% heat-inactivated fetal bovine serum (FBS; Cellmax, SA211.02, Beijing, China) and 1% penicillin/streptomycin (P/S, Gibco, 15140–122, Waltham, MA, USA) under standard conditions: a humidified incubator with 5% CO2 at 37 °C.

RNA isolation and real-time quantitative PCR (RT-qPCR): Total RNA was extracted from HCC tissues and cell lines using TRIeasy reagent (Yeasen, Shanghai, China), and its concentration and purity were assessed with a NanoDrop 2000 spectrophotometer (Thermo Fisher Scientific). For mRNA transcripts, first-strand cDNA was synthesized using the Hifair® 1st Strand cDNA Synthesis SuperMix (Yeasen, Shanghai, China). RT-qPCR was performed using the Hifair® III One Step RT-qPCR SYBR Green Kit (Yeasen, Shanghai, China) on a CFX Connect Real-Time PCR Detection System (Bio-Rad, CA, USA). The relative expression levels of mRNA were determined using the 2–ΔΔCt method, with GAPDH as internal controls, respectively. The primer sequences used in this study are provided in Supplementary Table S3.

Plasmids, retroviral infection and transfection: INPP4B and ALKBH5 full-length/mutant cDNA fragments were amplified via PCR and cloned into the corresponding vectors using specific primers. Targeted shRNA sequences were chemically synthesized and inserted into

pLKO.1 vectors by Tsingke Biotechnology. Plasmids were co-transfected with psPAX2 and PMD2.G packaging plasmids into 293T cells using ZETA Life's transfection reagent. Viral supernatants harvested at 48 h post-transfection were used to infect target cells supplemented with 10 μg/mL polybrene. Stable transductants were selected with 2 μg/mL puromycin for 10 days. Primer sequences and shRNA constructs are detailed in Supplementary Table S3.

Cell colony formation and proliferation assays: Pre-OB cells were cultured to 80% confluence, after which the medium was replaced with fresh medium, and the conditioned medium (CM) was collected following an additional 24 h of incubation and filtered through a 0.22 μm membrane. For the anchorage-dependent survival assay, HCC cells were seeded at a density of 2×10^2 cells per well into 6-well plates and cultured in fresh pre-OBs CM for 14 days, with the medium replaced every three days. After incubation, the cells were fixed with 4% paraformaldehyde for 20 minutes, stained with 0.5% crystal violet for 15 minutes, and gently rinsed with PBS to remove excess dye. Images were taken, and colonies of at least 50 cells each were counted manually. For the growth curve assays, HCC cells were seeded at a density of 5×10^3 cells per well into 96-well plates and cultured in fresh pre-OBs CM. Cell proliferation was assessed daily for 5 days using a standard cell counting kit-8 (CCK-8) assay (Yeasen, Shanghai, China). Absorbance at 450 nm was measured using a microplate reader (BioTek Instruments, Winooski, USA) to generate growth curves.

Western Blot Assay: Proteins from HCC tissues or cell lines were extracted using RIPA lysis buffer supplemented with phenylmethylsulfonyl fluoride (PMSF) and phosphatase inhibitors (Solarbio, Beijing, China). The protein lysates were then mixed with 5× SDS loading buffer and heated at 100°C for 10 minutes to induce protein denaturation. Equal amounts of protein samples were electrophoresed through SDS-PAGE, transferred to PVDF membranes (Millipore, Massachusetts, USA), and subsequently blocked with 10% non-fat milk at room temperature for 2 h. After blocking, the membranes were incubated overnight at 4°C with primary antibodies targeting the specific proteins, followed by incubation for 1 hour at room temperature with HRP-conjugated secondary antibodies. The protein bands were visualized using enhanced chemiluminescence (ECL) substrate, and the emitted signals were subsequently captured with an imaging system (Bio-Rad, USA). The anti-β-actin antibody served as an endogenous control, with the details of the primary antibody provided in

Supplementary Table S3.

Immunohistochemistry and histology: At experimental termination, hindlimb bones (tibiae/femora) were harvested, fixed in 4% paraformaldehyde, and decalcified in 12% EDTA (37°C, 10-14 days). Following decalcification, samples underwent graded ethanol dehydration, paraffin embedding, and 5-μm sectioning. Histopathological assessment included H&E staining for metastatic lesion characterization and TRAP staining (Sigma-Aldrich, 387A-1KT) to identify osteoclasts. IHC analysis evaluated CTSK and OCN expression through citrate buffer (pH 6.0)-mediated antigen retrieval, followed by H2O2 blocking, BSA incubation, overnight primary antibody incubation (4°C), and HRP-conjugated secondary antibody detection. DAB (ZSGB Bio) visualization was performed with hematoxylin counterstaining. Quantitative analysis of staining was performed by calculating the IHC score, which was determined as the product of staining intensity (0, no staining; 1, light yellow; 2, brown; 3, brownish red) and the percentage of positively stained cells (0, no positive cells; 1, <10%; 2, 10%-49%; 3, 50%-79%; 4, >80%).

Fluorescence in situ hybridization (FISH) and Immunofluorescence (IF) staining: FISH was performed to visualize tRF-1^{ArgACG} localization in HCC cells using Cy3-labeled probes (TsingkeBiotechnology, Beijing, China). Cells seeded on sterile coverslips (24-well plates) were fixed with 4% paraformaldehyde, permeabilized with 0.1% Triton X-100, and prehybridized in buffer at 37°C. Overnight hybridization (37°C, humidified chamber) used 10 nM Cy3-probes followed by stringent washing with 2×/1× SSC. Immunofluorescence utilized goat anti-rabbit IgG-Alexa Fluor 488 (ProteinTech, 1:250) after blocking with 10% goat serum in PBST. Slides were mounted with DAPI-containing anti-fade medium (Beyotime, Shanghai) and imaged via Olympus fluorescence microscopy (Tokyo, Japan).

Bone-in-Culture Array (BICA): Eight-week-old C57BL/6 mice were used for the BICA assay. After euthanasia, the femur and tibia were aseptically harvested from mice. The bones were cut into small fragments and placed into low-adsorption 48-well plates. Subsequently, 2 × 10^4 cells were seeded into each well and incubated at 37 °C for 24 h. After incubation, the wells were thoroughly washed with PBS to remove unattached tumor cells. Bioluminescence signals of tumor cells colonizing the bone tissues were measured using the IVIS Lumina II imaging system (PerkinElmer) at 4- and 7-days post-seeding. All bioluminescence data were

analyzed using Living Image software (PerkinElmer).

RNA sequencing (RNA-seq): After transfection of HCCLM3 cells with either tRF-1^{ArgACG} or NC for 48 h, total RNA was extracted using TRIeasy reagent (Yeasen, Shanghai, China) according to the manufacturer's protocol to ensure high RNA purity and integrity. Library construction and RNA-seq analysis were performed by Novogene Co., Ltd. (Beijing, China) using the Illumina NovaSeq 6000 platform (Illumina, USA), which led to the identification of differentially expressed genes (DEGs) between the two groups. The criteria for DEGs were defined as $|\log2(\text{FoldChange})| > 1$ and an adjusted p-value < 0.05.

Sucrose Gradient Fractionation Assay: Polysome profiling was performed as previously described (PMID: 32917240) with minor modifications. HCC cells treated with tRF-1^{ArgACG} or its inhibitor were cultured for 48 h in 10-cm dishes, followed by incubation with 100 μg/mL cycloheximide (CHX) for 15 min and two washes with ice-cold PBS. Cells were lysed in 500 μL of lysis buffer (5 mM Tris-HCl, pH 7.5; 2.5 mM $MgCl_2$; 1.5 mM KCl; 0.5% Triton X-100; 0.5% sodium deoxycholate; 2 mM DTT; 1× protease inhibitor; 100 U RNase inhibitor; 100 μg/mL CHX) on ice for 15 min. Lysates were cleared by centrifugation at 13,000 × g for 10 min, and the supernatant was layered onto a 5–50% linear sucrose gradient prepared in ultracentrifuge tubes and stored at 4°C overnight. Gradients were centrifuged at 35,000 rpm for 4 h, and 0.6 mL fractions were collected from top to bottom. Absorbance at 254 nm was measured to generate polysome profiles. RNA from each fraction was subsequently extracted using TRIzol LS Reagent, and distribution curves were plotted to assess ribosome occupancy.

RNA pulldown and mass spectrometry: Biotin-labeled tRF-1^{ArgACG} probe and control probe were synthesized by Henan Ruiying Biotechnology Co., Ltd. (Zhengzhou, China). RNA pull-down assays were performed according to the manufacturer's guidelines using the RNA pull-down kit (BersinBio, Guangzhou, China). Biotin-labeled tRF-1^{ArgACG} probe and control probe were incubated with whole-cell extracts from HCC cells, followed by the addition of streptavidin magnetic beads to capture the RNA-protein complexes. After extensive washing to remove non-specific binding, the complexes were eluted with protein elution buffer and subjected to SDS-PAGE for protein separation. The gel was stained with silver staining to visualize the protein bands. Finally, the protein bands were excised and subjected to mass spectrometry analysis at Bioprofile Co., Ltd. (Shanghai, China).

RNA immunoprecipitation (RIP) assay: In brief, 1×10^7 HCC cells were initially collected and lysed using RIP lysis buffer, which contained 150 mM KCl, 1 mM NaF, 2 mM EDTA-NaOH (pH 8.0), 50 mM HEPES-KOH, 0.5 mM DTT, 0.5% NP-40, 1× protease inhibitor cocktail, and 1 μl/ml RNase inhibitor. After incubation on ice for 15 minutes, the cell lysate was centrifuged at 13,000 × g for 15 minutes, and the supernatants were collected. Protein A/G magnetic beads (MCE, HY-K0202) were washed with RIP wash buffer and incubated with either specific antibodies or IgG control. The collected supernatants were combined with the beads-antibody complex and incubated overnight at 4°C with gentle rotation. The RNA-protein complexes were then treated with proteinase K buffer to degrade the proteins, followed by RNA purification using standard extraction methods to prepare the RNA for RT-qPCR analysis.

RNA stability assays: HCC cells were seeded into 6-well plates and cultured until reaching 70-80% confluence, after which actinomycin D (MCE, HY-17559, 5 μg/mL) was added to inhibit transcription. Cells were harvested at predetermined time points of 0, 3, 6, 9, and 12 h. RNA was extracted, and the expression levels of target genes at different time points were measured using qRT-PCR to compare their degradation rates.

ALKBH5 demethylase activity assay: The effect of tRF-1^{ArgACG} on ALKBH5 demethylase activity was evaluated using a cell-free assay with the Epigenase m⁶A Demethylase Activity/Inhibition Assay Kit (P-9013, EpiGentek, USA), with modifications based on previously described methods. Briefly, equal amounts of purified recombinant human ALKBH5 protein were incubated with synthetic wild-type (WT) tRF-1^{ArgACG}, U3A, U16A, U3A/U16A mutant. The mixtures were subsequently incubated with the m⁶A substrate in a 50-μL demethylation reaction containing Fe^{2+}, α-ketoglutarate, L-ascorbic acid, and the indicated reaction buffer. After incubation for 2 h, ALKBH5 demethylase activity was colorimetrically quantified at 450 nm using a microplate reader according to the manufacturer's instructions.

m6A dot blot assay: Total RNA extracted from HCC cells was denatured at 65°C for 5 minutes and immediately placed on ice. Approximately 200 ng of denatured RNA, dissolved in ice-cold SSC buffer, was spotted onto an Amersham Hybond-N+ membrane (GE Healthcare, USA). Ultraviolet (UV) crosslinking was then carried out for 10 minutes using a

UV cross-linker. To confirm RNA loading, the membrane was stained with 0.02% methylene blue (Solarbio, China) at room temperature for 5 minutes. After staining, the membrane was rinsed with RNase-free water to remove excess dye and imaged. The membrane was blocked with 5% non-fat milk at room temperature for 1 hour, followed by overnight incubation at 4°C with the m6A methylation antibody (1:600, proteintech). After appropriate washing, the membrane was incubated at room temperature for 1 hour with HRP-labeled goat anti-mouse IgG (H+L) (1:2000, Beyotime, Shanghai, China). Finally, the chemiluminescent signal was detected using an ECL substrate and captured with an imaging system.

Luciferase reporter assay: By replacing adenine (A) with cytosine (C) at the m6A modification sites, we synthesized the mutant (MUT1-MUT6) and wild-type INPP4B sequences and inserted them into the pmirGLO reporter gene vector, respectively. HCC cells were seeded into 24-well plates and subsequently co-transfected with the above luciferase reporter plasmids together with either shALKBH5 or OE-ALKBH5 plasmids. Firefly and Renilla luciferase activities were assessed 24 h post-transfection using the Luciferase Reporter Assay System (Yeasen, Shanghai, China) according to the manufacturer's protocol. The corresponding primer sequences are provided in Supplementary Table S3.